



Degradation of Sulfamethoxazole by Double Cylindrical Dielectric Barrier Discharge System combined with Ti /C-N-TiO₂ supported Nanocatalyst

Emile Salomon Massima Mouele, PhD^{a,m,*}, Tay Zar Myint Myo, PhD^b, Htet Htet Kyaw, PhD^c, Jimoh O Tijani, PhD^g, Mihaela Dinu, PhD^h, Anca C Parau, PhD^h, Iulian Pana, PhD^h, Youssef El Ouardi, PhD^m, Jamal Al-Sabahi, PhD^c, Mohammed Al-Belushi, MSc^e, Eduard Sosnin, PhD^j, Victor Tarasenko, PhDⁱ, Cheng Zhang, PhD^k, Tao Shao, PhD^k, Tanta Verona Iordache, PhD^l, Sandu Teodor, PhD^l, Katri Laatikainen, PhD^m, Alina Vladescu, PhD^{h,i}, Mohammed Al-Abri, PhD^{c,d}, Andrei Sarbu, PhD^l, Mariana Braic, PhD^h, Viorel Braic, PhD^h, Sergey Dobretsov, PhD^{e,f}, Leslie F Petrik, PhD^{a,*}

^a Environmental and Nano Sciences Group, Department of Chemistry, University of the Western Cape, Bellville, Cape Town 7535, Republic of South Africa

^b Department of Physics, College of Science, Sultan Qaboos University, P. O. Box 36, 123 Al-Khoud, Muscat 123, Sultanate of Oman

^c Nanotechnology Research Center, Sultan Qaboos University, P. O. Box 33, Al-Khoud, Muscat 123, Sultanate of Oman

^d Petroleum and Chemical Engineering Department, Sultan Qaboos University, P. O. Box 33, Al-Khoud, Muscat 123, Sultanate of Oman

^e Department of Marine Science and Fisheries, Sultan Qaboos University, P. O. Box 34, Al-Khoud, Muscat 123, Sultanate of Oman

^f Center of Excellence in Marine Biotechnology, Sultan Qaboos University, P. O. Box -50 Al-Khoud, Muscat 123, Sultanate of Oman

^g Department of Chemistry, Federal University of Technology, PMB 65, PO. Box 920 Minna, Niger State 920001, Nigeria

^h Research Center for Advanced Surface Processing and Analysis by Vacuum Technologies (ReCAST), National Institute for Research and development in Optoelectronics INOE 2000, Magurele, 077125 Bucharest, Romania

ⁱ Physical Materials Science and Composite Materials Centre, Research School of Chemistry & Applied Biomedical Sciences, National Research Tomsk Polytechnic University, Lenin Avenue 43, 634050 Tomsk, Russia

^j Institute of High Current Electronics, Russian Academy of Sciences, 2/3 Akademicheskoy Avenue, Tomsk 634055, Russia

^k Beijing International S&T Cooperation Base for Plasma Science and Energy Conversion, Institute of Electrical Engineering, Chinese Academy of Sciences, Beijing 100190, China

^l National Institute for Research and Development in Chemistry and Petrochemistry – ICECHIM Bucharest, 202 Spl. Independentei, 060021 Bucharest, Romania

^m Lappeenranta-Lahti University of Technology LUT, Department of Separation Science, P.O. Box 20, FI-53851 Lappeenranta, Finland

ARTICLE INFO

Keywords:

Wastewater
DCDBD
degradation efficiency
mineralisation
PPPs, photocatalyst

ABSTRACT

The presence and detection of persistent pharmaceutical pollutants (PPPs) in aquatic environments requires urgent remediation. C-N-TiO₂ was prepared by sol-gel method and immobilised on Ti mesh by dip-coating technique followed by pyrolysis in the furnace at 350°C for 105 minutes. The Ti/C-N-TiO₂ photocatalyst were characterised by SEM, EDS, XRD, Raman spectroscopy, and XPS. An optimised DCDBD system alone or combined with Ti/C-N-TiO₂ catalysts were compared for the degradation of sulfamethoxazole (SMX) simulated wastewater at the applied conditions. The SEM-EDS results showed that C, N, and Ti were all present in the C-N-TiO₂ nano catalyst layer supported upon Ti mesh. XPS results revealed existence of Ti in +4 oxidation states despite the addition carbon and nitrogen. The XRD and Raman patterns confirmed the formation of anatase as dominant phase. The antibacterial tests of Ti/C-N-TiO₂ films showed an excellent effect on *E. coli* inhibition. The degradation of SMX with DCDBD and DCDBD/C-N-TiO₂/Ti-mesh systems followed first-order reaction and complete mineralisation of

* Corresponding author at: Environmental Nano Science Research Group, Department of Chemistry, University of the Western Cape, Bellville, Cape Town 7535, South Africa.

E-mail addresses: emilemassima@yahoo.fr (E.S. Massima Mouele), myotayzar.myint@gmail.com (T.Z. Myint Myo), htethtetkyaw2006@gmail.com (H.H. Kyaw), jimohishola8@gmail.com (J.O. Tijani), mihaela.dinu@inoe.ro (M. Dinu), anca.parau@inoe.ro (A.C. Parau), iulian.pana@inoe.ro (I. Pana), uceef.elouardi@gmail.com (Y. El Ouardi), jamal@squ.edu.om (J. Al-Sabahi), hamoodbeluch@gmail.com (M. Al-Belushi), badik@loi.hcei.tsc.ru (E. Sosnin), vft@loi.hcei.tsc.ru (V. Tarasenko), zhangcheng@mail.iee.ac.cn (C. Zhang), st@mail.iee.ac.cn (T. Shao), iordachev.icechim@gmail.com (T.V. Iordache), sandu_m_teo@yahoo.com (S. Teodor), katri.laatikainen@lut.fi (K. Laatikainen), alinava@inoe.ro (A. Vladescu), alabri@squ.edu.om (M. Al-Abri), andr.sarbu@gmail.com (A. Sarbu), mariana.braic@inoe.ro (M. Braic), viorel.braic@inoe.ro (V. Braic), sergey@squ.edu.om (S. Dobretsov), lpetrik@uwc.ac.za (L.F. Petrik).

<https://doi.org/10.1016/j.hazadv.2022.100051>

Received 1 December 2021; Received in revised form 5 February 2022; Accepted 10 February 2022

2772-4166/© 2022 The Author(s). Published by Elsevier B.V. This is an open access article under the CC BY-NC-ND license

(<http://creativecommons.org/licenses/by-nc-nd/4.0/>)

the pollutants was achieved after 30 and 60 min of plasma run at rate constants of $3.79 \times 10^{-2} \text{ min}^{-1}$ ($R^2 = 0.999$) and $2.18 \times 10^{-2} \text{ min}^{-1}$ ($R^2 = 0.997$), respectively. The energy yield G_{50} required for the degradation of 50% SMX reached 34.64 g/kWh corresponding to an electrical efficiency per order (EE/O) of 40.527 kWh/m³ order¹ with DCDBD alone within 18 min, and 19.787 g/kWh with DCDBD/Ti/C-N-TiO₂ system corresponding to an EE/O of 70.458 kWh/m³ order¹ after 32 min. Different recalcitrant degradation intermediate by-products were detected by HPLC/MS and their degradation pathways proposed. Therefore, this study offers a novel advanced oxidation technology for the remediation of SMX from aqueous solution.

1. Introduction

The continuous identification and detection of persistent organic pollutants (POPs), a class of chemicals of emerging concern (CECs); in different water and wastewater sources has raised global concerns on environmental pollution and health issues. The most common CECs documented in the literature include pharmaceuticals, endocrine-disrupting compounds (EDCs), antibiotics, non-steroidal anti-inflammatory drugs (NSAIDs), and antiretroviral medicaments (Kusic et al., 2006, Koparal et al., 2007, Kishimoto et al., 2005, de O. Souza et al., 2021). Many of these POPs are considered carcinogenic owing to their biological effects which also include chronic noxiousness, causing endocrine disorder, and antibacterial resistance (Shu and Huang, 1995, Gupta et al., 2007, Suzuki et al., 2001, Spadaro et al., 1992, Mozia et al., 2005).

Pharmaceutical residues have long been detected in water and wastewater treatment plants (WWTPs) at low concentrations and are often below the detection limits of less sensitive analytical equipment (Krishnan et al., 2021). These substances originate from various sources including medicines, personal hygiene products, and cosmetics, livestock farming, aquaculture to mention but a few, and thus found to accumulate in diverse environmental media (Mhuka et al., 2020). The occurrence of pharmaceutical in aquatic media have compromised water and wastewater quality (Olatunde et al., 2020, Mhuka et al., 2020, Dhanke et al., 2018). These compounds are highly mobile, persistent and escape from water treatment facilities into the environment (Nam et al., 2001, Massima Mouele et al., 2021).

Sulfamethoxazole (SMX) is one of the antibiotics used for the treatment of various bacterial infections such as urine track, respiratory, and intestinal infections to only cite a few. Its high consumption has led to an increase in its demand and continuous manufacturing by pharmaceutical industries (Wang et al., 2011). Its abundance and persistence in the tertiary treatment stage of water and wastewater treatment facilities have raised serious environmental concern, and hence its removal from water bodies requires urgent attention (Dimitrakopoulou et al., 2012, de A.G.U. de Souza et al., 2010).

Due to their low concentrations, the removal of SMX is often achieved at the tertiary wastewater treatment stage that involves various processes such as photo-degradation, photo-Fenton, photocatalysis, photolysis, chlorination, ozonation, advanced oxidation processes (AOPs), and advanced reduction process (Olatunde et al., 2020). However, these methods require extensive wet chemistry, high cost, and generate significant amounts of secondary wastes. AOPs in their various configurations produce non-selective hydroxyl radicals and co-species that directly or indirectly mineralise the targeted organic or inorganic contaminants (de A.G.U. de Souza et al., 2010). The most common AOPs previously reported include O₃/H₂O₂, O₃/UV, UV/TiO₂ and UV/TiO₂/O₃, UV/H₂O₂, TiO₂/UV, and TiO₂/UV/H₂O₂, O₃/UV/H₂O₂ among others (Madhu et al., 2009, Iqbal et al., 2013). Though these combinations have been found suitable for water and wastewater remediation, Mouele et al. (2021) opined that the excessive use of powder catalysts usually obscures the penetration of UV light, and the highly oxidative environment damaged catalyst supports, other problems such as poor mixing causes ozone leakage, thus hinders the applicability of

AOPs based on powder catalysts in water and wastewater treatment. Nevertheless, in the last decades, the use of semiconductors heterogeneous photocatalysts such as TiO₂ and its modified forms as supplementary technologies toward boosting the production of OH[•] for complete mineralisation of wastewater contaminants like pharmaceuticals, and microorganisms have attracted significant interest worldwide (Adewuyi, 2005, Chan et al., 2011). TiO₂ has been widely studied and preferred due to its photochemical stability, excellent oxidising capacity, and enhanced antimicrobial efficacy (Patil et al., 2018, Patil et al., 2020). On the other hand, post-separation of powder TiO₂ photocatalyst from treatment poses limitations that can be overcome by suspension of the catalysts on various supports such as mesh, glass, zeolite, clay, activated carbon (Mouele et al., 2020a, Mouele et al., 2020b). In addition, TiO₂ catalysts have previously been immobilised on stainless steel (SS) mesh however, corrosion of SS-mesh support was experienced and needed to be overcome (Hu and Wang, 2021, Massima Mouele et al., 2020).

Unlike other systems, AOPs induced by non-plasma technologies with diverse electrode geometries have been found effective to degrade water toxins and related applications (Erofeev et al., 2019, Erofeev et al., 2020). However, the energy consumption and the limited lifespan of high voltage (HV) electrodes due to corrosion play a crucial role during the plasma treatment of water and wastewater (Ikehata et al., 2006, Klavarioti et al., 2009). Dielectric barrier discharge (DBD) is initiated with only 1 eV and HV electrodes that are covered by more than one dielectric material have been utilised as a convenient method for the decontamination of wastewater (Erofeev et al., 2020, Ikehata et al., 2006, Klavarioti et al., 2009). Various authors established that the combination of AOPs effectively detoxified water containing organic pollutants than a single AOP system (Kalumuck and Chahine, 2000, Wang et al., 2009, Wang et al., 2010). DBD generates UV light, shock waves, and various ROS such as O₃, H₂O₂, O[•], O₂⁻, OH[•], etc. and reactive nitrogen species (RNS) and can be applied as a combination of several AOPs (O₃/H₂O₂, UV/O₃, UV/H₂O₂, UV/O₃/H₂O₂) for remediation of water and wastewater (Kalumuck and Chahine, 2000, Wang et al., 2009, Wang et al., 2010–(Miruka et al., 2021). Double cylindrical DBD (DCDBD) described by Mouele et al. (2020) combined with supported catalyst appear to be an adequate alternative.

Thus, in this study, the performance of an optimised DCDBD alone and DCDBD combined with Ti/C-N-TiO₂ mesh catalysts on the degradation of SMX pharmaceutical drug in aqueous solution was evaluated. Firstly, C-N-TiO₂ nano catalyst was synthesised by the sol-gel method and then immobilised on pure Ti mesh by dip coating. The coated Ti/C-N-TiO₂ meshes were pyrolysed at 350°C, using a ramping rate of 50°C/min, and held at temperature for 105 min under an N₂ flow of 20 mL/min. The resultant Ti/C-N-TiO₂ composites were characterised by SEM, XRD, Raman, and XPS. The antibacterial effect of Ti/C-N-TiO₂ films was investigated upon the inhibition of *E. coli* bacteria at the applied conditions. Thereafter, the degradation of the selected pollutant SMX by an optimised DCDBD system alone, and DCDBD system combined with Ti/C-N-TiO₂ films were investigated under the applied conditions. The transformation compounds of SMX were identified by HPLC-MS (LC-MS) and their degradation mechanistic pathways were suggested.

2. Material and methods

2.1. Materials

The chemicals used for the synthesis of carbon-nitrogen co-doped catalysts (C-N-TiO₂) included polyacrylonitrile (PAN) powder (99.5%, Good Fellow Cambridge Ltd., UK); titanium tetrachloride, (MW189.68 g/mol), titanium (IV) oxide (powder), Degussa (99.5%), sulfamethoxazole (AS) (SMX, Lot#BCBP8794V PCODE:101739693) were purchased from Sigma-Aldrich; N, N-dimethyl formamide (DMF) 99%; ammonium nitrate, (ACS (95%), Industrial Analytical (Pty), South Africa), and sulfuric acid (98%); sodium hydroxide flakes CP (97%, Kimix Airport Industrial, South Africa). The commercial pure Titanium meshes (12 cm x 2 cm, 2.5 cm diameter, 0.4 cm thickness) were purchased from Good Fellow, England. A magnetic stirrer Hei-Mix S-UK 230 V / 50 Hz with UK plug, (purchased from Laboratory Equipment South Africa, Athlone, Cape Town, 7760, South Africa) was used for sol-gel mixing, ceramic crucibles, a 3-zone horizontal ceramic tube furnace (Brother XD 1600M furnace (Brother XD 1600MT manufactured by Zhengzhou Brother Furnace Co, LNpt clear TD, Electronic Industrial Town Zhanggong Pu, Xiu wu county, Jiaozuo, China) and 805 cm furnace tube made in quartz connected to a nitrogen gas inlet with a flow set at 100 mL/min were used to pyrolyse the Ti/C-N-TiO₂ films under N₂ (99 %) flow. The equipment used in the DBD experimental protocols has been described in our previous work (Massima Mouele et al., 2020).

2.2. Experimental procedures

2.2.1. Preparation of C-N-TiO₂ sol-gel and immobilisation on uncoated Ti mesh

The preparation of C-N-TiO₂ sol-gel was achieved following the procedure described by Mouele et al. (2020), involving the mixture of polyacrylonitrile (PAN), N, N-dimethyl formamide (DMF), and ammonium nitrate (NH₄NO₃) followed by continuous stirring for 24 h at ambient temperature. Pure titanium (Ti) meshes were pre-treated with a solvent system consisting of acetone, ethanol, and water and were dried in an oven at 60°C for 30 min. The immobilisation of C-N-TiO₂ sol-gel on the cleaned and dried Ti was done by dip-coating followed by pyrolysis in the furnace at 350°C, using a temperature ramping rate of 50°C/min, and held at temperature for 1 hour 45 minutes under an N₂ flow of 20 mL/min (Mouele et al., 2020).

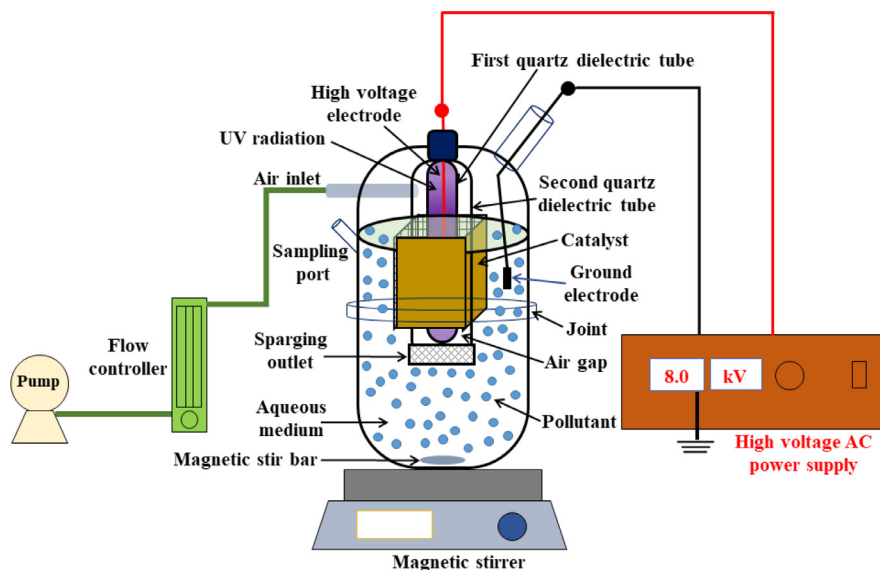


Fig. 1. Optimised double cylindrical DBD (DCDBD) reactor used for detoxification of SMX with Ti/C-N-TiO₂ catalyst at the following conditions: Applied voltage 8 kV, discharge power 60 W, current 60 mA, solution volume 1.5 L, airflow rate 3 L/min, 1.5 mm silver electrode, 50 g/L NaCl inner electrode-electrolyte, air gap 2 mm.

2.2.2. Characterisation of uncoated and C-N-TiO₂ coated Ti meshes and antibacterial activity

The characterisation of Ti/C-N-TiO₂ films was performed by various techniques including SEM, XRD, Raman spectroscopy, and XPS. The detailed procedures are provided in Text S1 in supplementary material; while the antibacterial activity and statistical analysis are described in Texts S2 and S3, respectively in the supplementary material.

2.2.3. Preparation of stock and standard solutions of SMX drug and high-performance liquid chromatography analysis

The preparation of stock and standard solutions of SMX drug is described in Text S4 while the high-performance liquid chromatography (HPLC) analysis of sulfamethoxazole and determination of degradation intermediate by-products method is provided in Text S5 in the supplementary material.

2.2.4. Description of the double cylindrical dielectric barrier discharge system

The double cylindrical dielectric barrier discharge (DCDBD) reactor is schemed in Fig.1, while its description is provided in Text S6 in the supplementary material.

2.2.5. Dielectric barrier discharge photochemical experimental procedure

The degradation of SMX (40 mg/L, pH 6.5) by the DCDBD system was achieved according to the procedure reported by Mouele et al. (2020). A high voltage electrode from an AC power supply set at a voltage of 8 kV, delivering a power of 60 W, and current of 60 mA, was connected to a 1.5 mm silver electrode that was directly immersed in a 50 g/L sodium chloride electrolyte in the inner tube of DCDBD reactor. The 23 cm long DCDBD reactor had a total volume capacity of 2 L, though the pollutant SMX volume was fixed at 1.5 L to avoid run-off of the solution and short circuits during DBD tests. An air compressor with an output of 60 L/min was connected to an airflow meter that was linked to the DCDBD reactor as a source of air/oxygen. Simulated SMX solutions at the indicated concentration were treated in the DCDBD system for 60 min (each experiment) and sampled every 10 min. From the initial concentrations and the linear trend $Y_1 = 10597X$ ($R^2 = 0.9995$), the final concentration of SMX was successfully estimated. The resultant degradation by-products of both pollutants were identified by HPLC-MS previously described in section 2.2.6. On the other hand, the photocatalytic degradation of SMX by DCDBD combined C-N-TiO₂ immobilised on pure Ti meshes is disclosed in Text S7 in the supplementary material.

3. Results and discussion

3.1. Characterisation of the Ti/C-N-TiO₂ supported catalyst

3.1.1. Scanning electron microscopy and energy dispersive spectroscopy of Ti/C-N-TiO₂ films

The morphology and elemental composition of the Ti/C-N-TiO₂ coating were investigated using scanning electron microscopy coupled with energy dispersive spectroscopy (SEM-EDS) and the results are presented in Fig. 2(a & b) while the elemental composition of pure Ti meshes and coated Ti is shown in Table ST1 (supplementary material) Fig. 2. (a & b) show that C-N-TiO₂ was effectively immobilised on pure Ti mesh. The uncoated Ti mesh in SEM micrograph Fig. 2 (a) was covered during the dip coating and pyrolysis protocol by the catalyst resulting in the coating in Fig. 2 (b) demonstrating excellent adherence between the catalysts and Ti support. The SEM micrograph in Fig. 2 (b) indicates the formation of a porous C-N-TiO₂ nanocatalyst layer on the coated Ti mesh with minuscule, compressed nanocrystals which corroborate the outcomes of Mouele et al. (2020) and Çomakli et al. (2014). In compar-

ison with literature, Zhang et al. (2003) prepared mesoporous TiO₂ film photocatalysts immobilised on stainless steel support by the sol-gel technique using Ti (OC₄H₉)₄ as a precursor and polyethylene glycol (PEG) as a structure-directing agent showed that the synthesised TiO₂ film was mesoporous. Various authors (Liao et al., 2012, Souzanchi et al., 2013, Merajin et al., 2013, Krýsa et al., 2014) claimed that the mesoporosity of nanomaterials influences the photocatalytic activity/properties of the coated catalysts. This agrees with the findings of Çomakli et al. (2016), and Zhang et al. (2016). Table ST1 (supplementary materials) shows the elemental composition (W %) of uncoated and C-N-TiO₂ coated Ti meshes by EDS. It was noticed that the amount of C in uncoated Ti mesh itself was 3.86% and then increased to 4.07% in the C-N-TiO₂ coated Ti, while Ti content was 51.64% in the uncoated Ti mesh increased to 53.2% in the C-N-TiO₂ coated Ti mesh. The C impurity detected in uncoated Ti mesh was probably due to the C stickers used to carbon coat the sample before SEM analysis. Moreover, the EDS showed that an additional 0.21% of C was detected in the co-doped C-N-TiO₂ showing that C was featured in the prepared nanocomposites. Likewise, the increase of Ti content from 51.64% in the uncoated Ti mesh to 53.2% in the

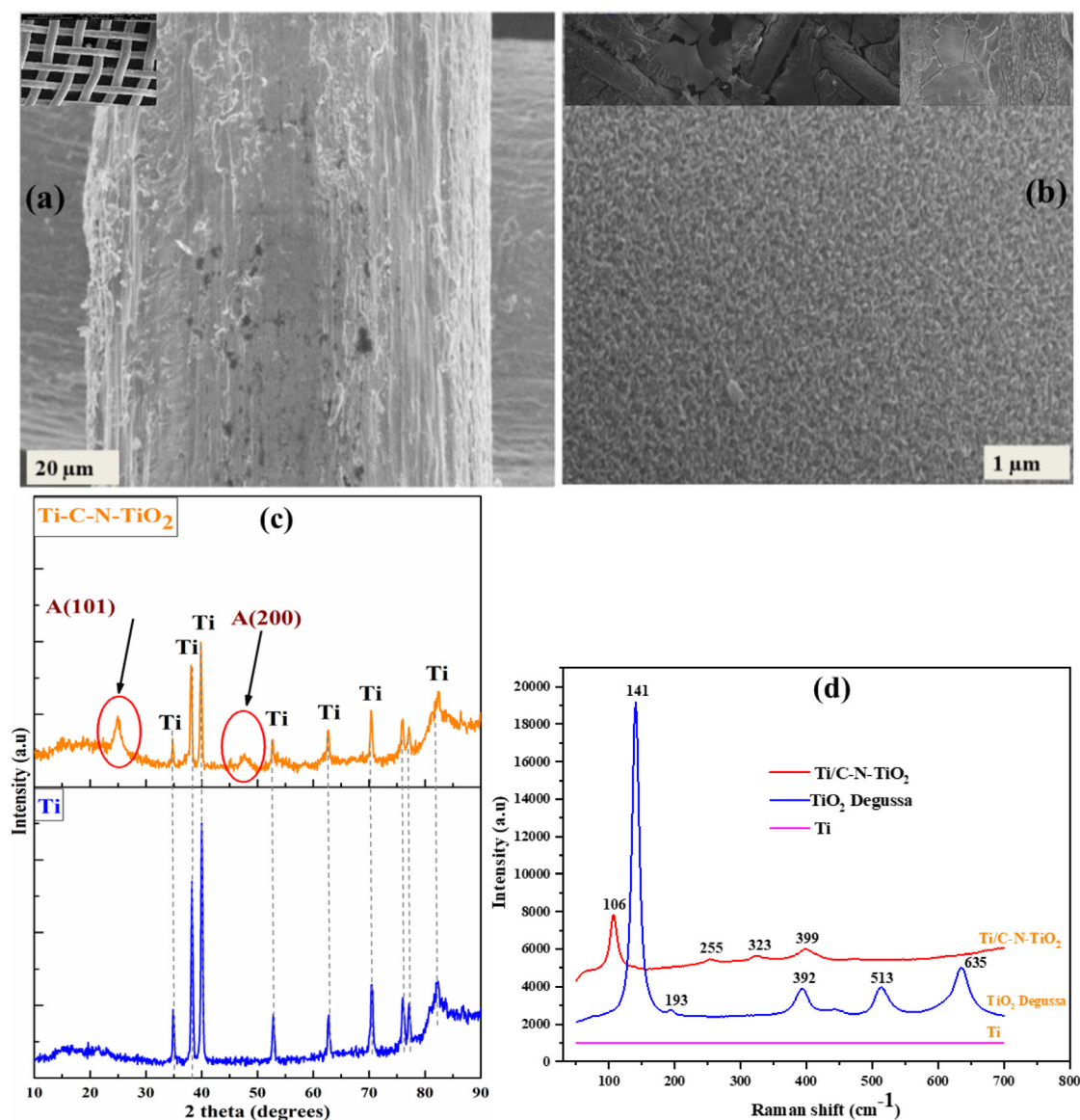


Fig. 2. SEM micrographs of (a) single line from pure Ti mesh (Inset: Pure Ti mesh) and (b) Magnified image of Ti/C-N-TiO₂ catalyst coating (Inset: Ti/C-N-TiO₂ catalyst mesh), and X-ray diffraction patterns (c), and Raman analysis (d) of Ti/C-N-TiO₂ supported catalysts pyrolyzed at 350°C, a ramping rate of 50°C/min for 105 min; Ti = pure titanium mesh, A= anatase.

Ti/C-N-TiO₂, respectively showed that Ti was also encountered in the supported nanocatalyst. So, the traceable amounts of C in uncoated Ti mesh was 3.86%, while that of Ti/C-N-TiO₂ was found to be 4.07% after coating, show a slight increase of C content in the prepares C-N-TiO₂ nanocatalyst, and a similar tendency was detected with Ti content that was 51.64% in the uncoated Ti mesh and which increased to 53.2% in Ti/C-N-TiO₂ after coating, showing that approximately 1.56% of Ti content originated from the engineered C-N-TiO₂ nano catalysts. Therefore, these results justify the different morphological aspects observed in Ti/C-N-TiO₂ catalysts in the SEM images shown in Fig. 2 (a & b) and those reported by Zhang et al. (2016) and Yetim (2016)).

3.1.2. X-ray diffraction and Raman spectroscopy analysis of the synthesized Ti/C-N-TiO₂ catalysts

The XRD pattern and Raman spectroscopy analyses were employed to define the phase composition, particle size, and the crystallinity of C-N-TiO₂ co-doped nanoparticles immobilised on pure Ti mesh (Ti/C-N-TiO₂), and the results are shown in Fig. 2(c & d) Fig. 2.c indicates that co-doped C-N-TiO₂ solely and predominantly comprised anatase phase (JCPDS, No. 00-021-1272) with the broadness and minimal intensities of peaks, an indication of small crystallite size of the catalyst coated C-N-TiO₂ (Table ST2, supplementary material). The diffraction peaks appearing at $2\theta = 35, 38, 39, 53, 63, 70, 77, 78, 83^\circ$ correspond to the alpha-phase of pure Ti mesh (α -Ti) and/or to O-Ti-O framework to some extent, which is consistent with previous studies (Zhang et al., 2016, Yetim, 2016, Omakli et al., 2015). In addition, the following diffraction peaks at 2θ values of 25.28° (101) and 48° (200), corresponding to the body-centered tetragonal lattice structure of the pure mineral anatase phase of C-N-TiO₂ (Mouele et al., 2020). Moreover, Raman spectra in Fig. 2(d) indicate that the most featuring peak of TiO₂ Degussa at 141 cm^{-1} and those appearing at $392, 513, 635\text{ cm}^{-1}$ validate the anatase phase of powder TiO₂ catalyst. However, these characteristic peaks of the anatase phase shifted to the left in the case of Ti/C-N-TiO₂ coating. In this regard, the intensity of peaks significantly decreased in a broadening fashion. Consequently, the dominant C-N-TiO₂ peak depicted at 106 cm^{-1} and the minor features identified at $255, 323, \text{ and } 399\text{ cm}^{-1}$ supported the anatase phase observed in Fig.2c.

3.1.3. XPS analysis of C-N-TiO₂ catalysts on Ti-mesh

Fig. 3 (a-d) shows the surface composition and chemical states of C-N-TiO₂ catalysts calcined at 350°C for 105 min on Ti-mesh. As a comparison, XPS spectra of pure Ti-mesh are also included in Fig. 3 (a-c). From the survey spectra (Fig.3a), titanium, carbon, and oxygen peaks can be observed from C-N-TiO₂ catalysts on Ti-mesh as well as pure Ti-mesh. The distinct N 1s peak appears at a binding energy of $\sim 400\text{ eV}$ which affirmed the presence of C-N-TiO₂ catalysts on Ti-mesh. Additionally, an increase in the binding energy of C 1s, Ti 2p, and O 1s peaks is observed in C-N-TiO₂ on Ti-mesh Fig. 3.b shows the high-resolution scan of C 1s and three components can be assigned to C-C/C-H at 284.6 eV , C-O at 285.3 eV , and C-O-C at 286.5 eV for pristine Ti-mesh and C-C/C-H at 284.6 eV , C-O at 285.9 eV , and C=N at 287.2 eV for Ti/C-N-TiO₂ catalyst mesh respectively (Wang et al., 2015, Zhang and Xing, 2018). High-resolution spectra in Fig. 3c show the core level binding energy of Ti 2p_{3/2} and Ti 2p_{1/2} where the peak positions at 457.6 eV and 463.4 eV can be assigned to pristine Ti-mesh and at 458.6 eV and 464.3 eV for Ti/C-N-TiO₂ with a spin-orbit splitting of $\sim 5.8\text{ eV}$ (Wu and Wang, 2013, Ren et al., 2015). Ti 2p peak from Ti/C-N-TiO₂ fled to a higher binding energy value of $\sim 1.0\text{ eV}$ compared to pristine Ti-mesh and the observed positive binding energy shift was attributed to the interaction of catalysts with Ti-mesh. The deconvoluted high-resolution N 1s of Ti/C-N-TiO₂ in Fig. 3d reveals the existence of two peaks at 398.5 eV and 399.9 eV and can be associated with N atoms in O-Ti-N linkages and C=N-C in pyridine N respectively (Ghazzal et al., 2014, Wang et al., 2017).

3.2. Antimicrobial test/activity of Ti/C-N-TiO₂ coating on E. coli

Fig. 4 shows the antimicrobial activity of C-N-TiO₂ catalysts supported on Ti mesh (Ti/C-N-TiO₂), and Ti mesh (control) in the dark (a) and under visible light (b) after 48 h. The statistical analysis (ANOVA) of these experiments is presented in Tables ST 3 and ST4 (supplementary material).

In the dark conditions, Ti/C-N-TiO₂ coating significantly (ANOVA, Tukey HSD, $p < 0.0005$) reduced the number of viable *E. coli* cells by 27.5% after 24 h when compared to the control Ti mesh (Fig. 4a). Nevertheless, a noticeable reduction of the number of CFUs of *E. coli* after 48 h in the same conditions (ANOVA, Tukey HSD, $p < 0.0005$) was observed for both coated and uncoated Ti meshes. The antibacterial effects of nanoscale TiO₂ have been reported earlier (Heinlaan et al., 2008). However, the toxicity of TiO₂ in the dark is weaker compared to other metal oxide nanoparticles (Heinlaan et al., 2008). Data shown in Fig. 4b indicate that in light conditions, Ti/C-N-TiO₂ exhibited significant antimicrobial activity against *E. coli* after both 24 and 48 h (ANOVA, Tukey HSD, $p < 0.0005$) as compared to Ti/control. The bactericidal effect of TiO₂ during irradiation is ascribed to the destructive impact of reactive oxygen species (ROS) such as O₂⁻, H₂O₂ and HO[•] resulting from the irradiation process on the cell walls of Gram-negative bacteria (Xiao et al., 2015, Zhang et al., 2016). Comparable and remarkable antimicrobial activity of Ti and TiO₂ against yeast (*Saccharomyces cerevisiae*), bacteria (*Lactobacillus acidophilus* and *Escherichia coli*), and green algae (*Chlorella Vulgaris*) under visible light irradiation have previously been reported (Karunakaran et al., 2010, Matsunaga et al., 1985). Various reports substantiate that OH[•] attack and the lipid peroxidation reaction are the principal reaction mechanisms governing the photocatalytic bactericidal effect of TiO₂ and are responsible for the destruction of *E. coli* cells (Kim and Kim, 2003, Maness et al., 1999, Gogniat et al., 2006). Co-doping of TiO₂ with C and N enhanced the photocatalytic performance of TiO₂ and increased the antimicrobial activity of Ti/C-N-TiO₂ coating. Li et al. (2008) reported that nitrogen-doped titanium dioxide (N-TiO₂) showed unimpeachable antimicrobial properties against gram-negative (*E. coli*) after 3 h exposure to visible light. This could be responsible for the exceptional antimicrobial properties of Ti/C-N-TiO₂ coating observed in Fig. 4 (b), suggesting that the co-doping of TiO₂ with C and N increased the hydrophilicity at the surface of the C-N-TiO₂ coated Ti mesh during visible-light irradiation. The statistical analysis (ANOVA) shown in Tables 1 & 2 reveals that both exposure time and the type of coating, as well as their combination, affected the number of viable *E. coli* cells.

The results dictated by SEM-EDS, XRD, Raman spectroscopy, and XPS analysis indicate that C-N-TiO₂ was successfully adherent on Ti mesh making it an excellent catalytic support. The Ti/C-N-TiO₂ films engineered show outstanding antibacterial activity which is an extended attribute of the coatings when applied as photocatalytic supports during treatment of water and wastewater. This, therefore, palliate the issue of post-separation of powder catalyst and killing of bacteria from treated effluents. Therefore, our investigation demonstrates that Ti/C-N-TiO₂ films not only possess antibacterial properties, but they are photo catalytically active with Ti mesh being suitable catalytic support. These data have not been reported elsewhere.

3.3. Degradation of SMX by DCDBD plasma reactor: impact of working parameters

The effect of working parameters of the DCDBD reactor, including initial concentration, solution pH, airflow rate, and applied voltage on the degradation percentage of SMX was evaluated at the applied conditions and the results are shown in Fig. 5. The influence of initial concentration and solution pH on SMX decomposition was investigated by varying SMX concentration from 20, 40, 60 to 100 mg/L and solution pH from 2.5, 6.5, 8.5 to 10 Fig. 5 (a & b) while other factors were kept constant at the applied conditions Fig. 5. (a & b) demonstrated that the

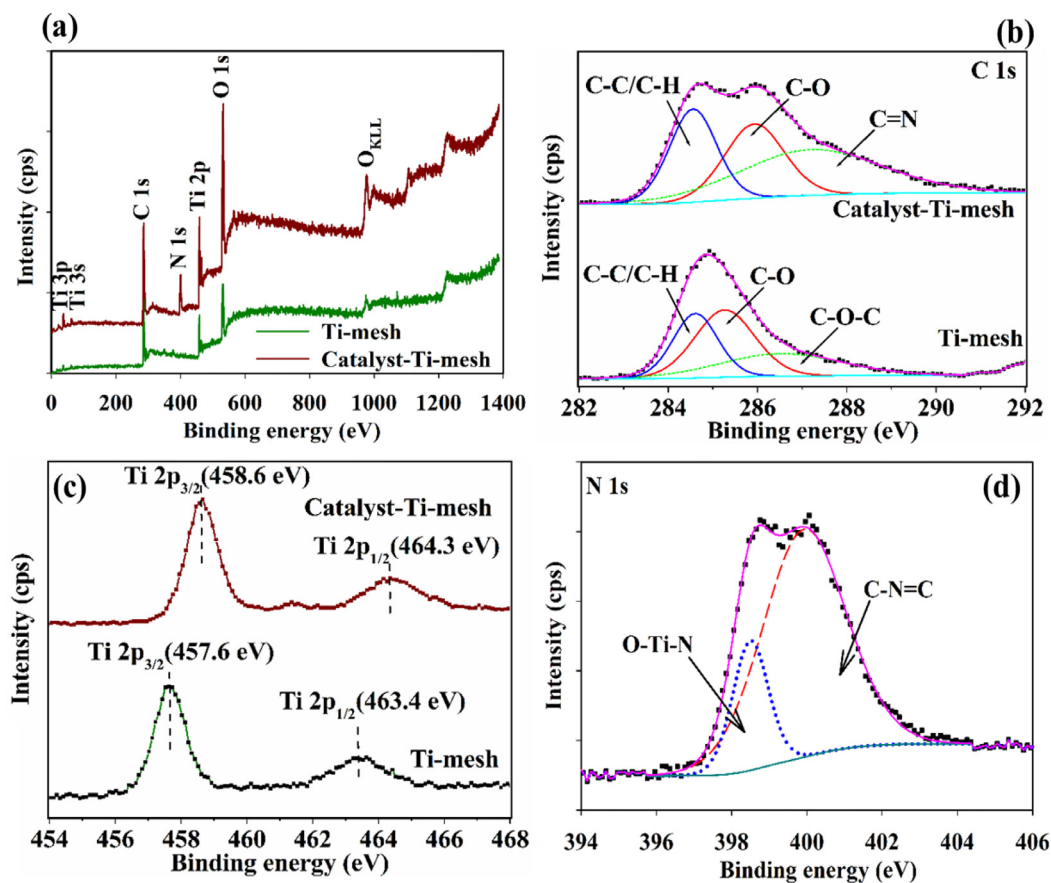


Fig. 3. (a) The XPS survey spectra, (b) high-resolution C 1s, (c) high-resolution Ti 2p and (d) high-resolution N 1s for Ti/C-N-TiO₂ catalysts coating calcined at 350 °C for 105 min.

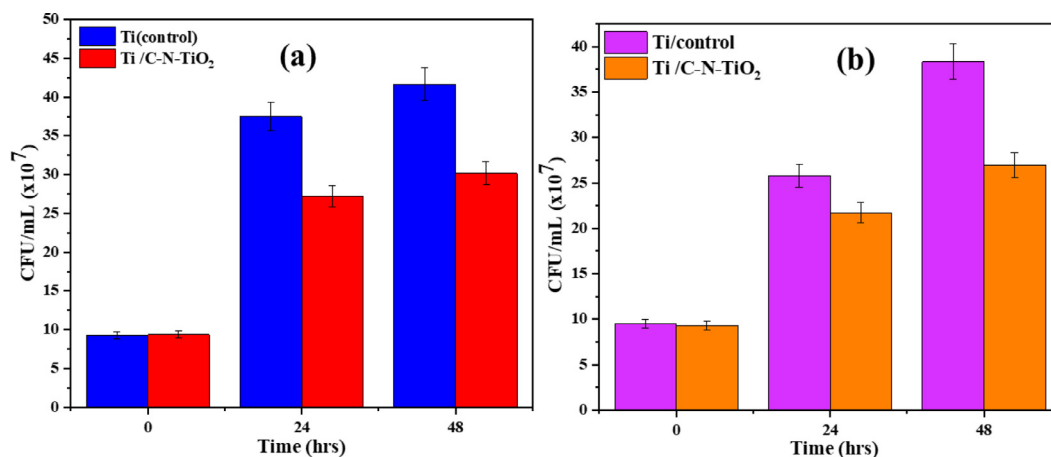


Fig. 4. The antimicrobial activity of pure titanium mesh (Ti)/control and C-N-TiO₂ coated catalysts mesh (Ti/C-N-TiO₂) in the dark (a), and under visible light (b) conditions after 48 h.

Table 1

ANOVA data for CFU comparisons during the antibacterial bioassay with *E. coli* and, under dark conditions. Time is the time of the experiment (0, 24 and 48 hours). Coatings refers to Ti/C-N-TiO₂ and uncoated Ti mesh (control).

E. coli/ Dark					
Intercept	Sum of Squares (SS)	Degree of Freedom (DF)	Mean square (MS)	F	p
Time	0.551624	1	0.551624	77496.01	0.000001
Coatings	0.007667	6	0.001278	179.52	0.000001
Time* Coatings	0.100148	2	0.050074	7034.76	0.000001
Error	0.050911	12	0.004243	596.03	0.000001
	0.000005	7	0.000007		

Table 2

ANOVA data for CFU comparisons during the antibacterial bioassay with *E. coli* under visible light conditions. Time is the time of the experiment (0, 24 and 48 h). Coatings refers to Ti/C-N-TiO₂ and uncoated Ti mesh (control).

E. coli/ Light					
Intercept	Sum of Squares (SS)	Degree of Freedom (DF)	Mean square (MS)	F	p
Time	0.526156	1	0.526156	610.7834	0.000001
Coatings	0.076234	2	0.038117	44.2476	0.000256
Time*Coatings	0.070200	9	0.007800	9.0545	0.007195
Error	0.046817	18	0.002601	3.0193	0.088340
	0.005169	6	0.000861		

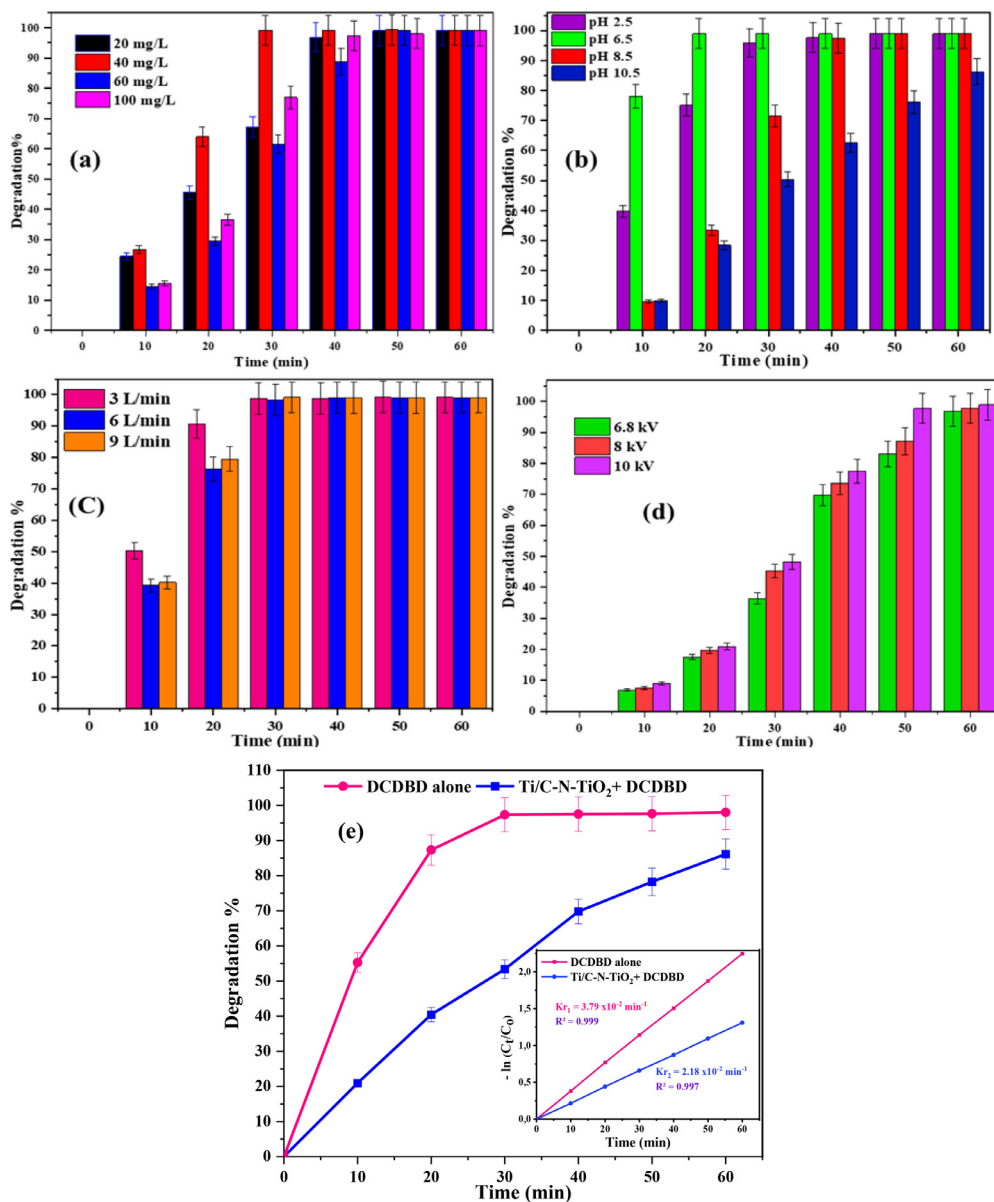
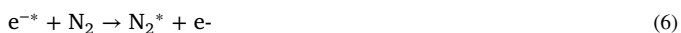


Fig. 5. Effect of working factors such as initial concentration (a), pH (b), airflow rate (c), and applied voltage (d) on the degradation of SMX in the DCDBD reactor, and (e) degradation of SMX by optimised DCDBD alone and DCDBD + Ti/C-N-TiO₂ supported catalysts at the following conditions: solution volume of 1.5 L, 1.5 mm silver electrode, 50 g/L NaCl electrolyte and 60 min of treatment time, (n = 2).

removal of SMX in the DCDBD system at different concentrations and solution pH (Fig. 5 a & b) did not follow constant trends but increased with prolonged treatment time. Nevertheless, complete SMX removal (99.99 %) in Fig. (5a) was achieved at a concentration of 40 mg/L after 30 min, while total degradation (99.99 %) of SMX in Fig. (5b) was attained at pH 4 after 20 min of DCDBD run, respectively. Likewise, Fig. (5b) shows that the highest removal of SMX was achieved in acidic media (< 7). These results show that pollutant initial concentration and solution pH play a crucial role in the treatment of pharmaceutical contaminated wastew-

ater. In addition, these results show that an optimised DCDBD reactor is an exceptionally advanced oxidation system suitable for the detoxification of SMX pharmaceutical pollutants at varied concentration and their corresponding pH. The variation of SMX oxidative percentages at different concentrations of pollutants given in Fig. 5a could be ascribed not only to the amount of reactive oxygen species (ROS) generated in the DCDBD reactor but also to their interaction with SMX pollutants (Wang et al., 2011). The abundant generation of ROS in DCDBD has previously been reviewed (Mouele et al., 2021, Mouele et al., 2015),

and their main production mechanisms are summarised in Eqs. (6)–(21). Their quantification in the DCDBD reactor was discussed in previous work (Massima Mouele et al., 2018, Massima Mouele et al., 2020).



Previous studies reported that O_3 is produced in acidic conditions with pH (< 7) and promptly reacts with unsaturated compounds/complexes (Mishra and Gogate, 2010, Gogate and Pandit, 2004, Kim et al., 2013), while the non-selective OH^{\bullet} is often considered inactive in acidic media, is generated in minor quantity (Stahelin and Hinge, 1985). This, therefore, implies that O_3 majorly reacted with SMX, and its metabolites accelerated the oxidation process compared to OH^{\bullet} whose interactions required extended time to achieve total oxidation. The different degradation percentages 99.99, 95.84, and 94.85% of SMX obtained in the DCDBD reactor alone with 40, 100, and 20 mg/L SMX after 40 min of plasma run at the applied conditions could imply that the degradation of SMX was concentration-dependent in the DCDBD reactor. In contrast, various authors (Glaze, 1986, He et al., 2014, Kuo et al., 2015) reported that total oxidation of by-products, for example, amides and amines, are resistant to O_3 in DBD acidic media, but are nevertheless weakened or often destroyed by OH^{\bullet} radicals (qiong Gao et al., 2012, Qi et al., 2014). Moreover, the detoxification of 60 mg/L SMX in the DCDBD reactor alone required 40 min to reach 86.79%. The literature presents little or no information on the impact of initial solution concentration on the degradation efficiency of SMX in the DCDBD system. However, a few authors (Wang et al., 2011, Beltrán et al., 2008, Dimitrakopoulou et al., 2012) noticed similar trends during an assessment of the effect of variation of initial concentration on the removal percentage of SMX using different treatment processes. Therefore, the total decomposition (99.99%) of 40 mg/L SMX reached after 30 min of DCDBD treatment indicates that the degradation metabolites obtained at this concentration were vulnerable to O_3 and related co-species attack, thus 40 mg/L was selected as the optimum concentration value used during the optimisation of DCDBD system.

Data plotted in Fig. 5 (c) shows that higher degradation of SMX was achieved at a lower air flow rate, while complete removal of the pollutant was reached after 30 min of DBD run. For instance, after 20 min of the experiment, 90.75 % of SMX degradation was achieved with an air flow of 3 L/min compared to 79.53 % and 76.42 % reached with 9 and 6 L/min, separately. These outcomes signify that at a lower airflow rate, reactive oxygen species/free radicals are effectively produced by various mechanistic pathways as previously claimed (Massima Mouele et al., 2021, Mouele et al., 2021). However, an increase in airflow rate in the DCDBD system interrupts the mechanistic pathways during ROS production for the formation of potent free radicals such as O_3 , H_2O_2 , and OH^{\bullet} and certainly reduced their amounts in the DCDBD reactor (Kim et al., 2013, Jiang et al., 2013). This consequently reduced the degradation of SMX at higher airflow rates. Similar trends were reported in previous studies conducted on the degradation of phenolic compounds using different plasma pulsed discharge configurations (Tri Sugiarto and Sato, 2001, Cheng et al., 2007, Bian et al., 2009). Their investigations claimed that enhanced degradation of phenols was achieved at gas flow rates less than or equal to 3 L/min. Subsequently, 3 L/min was chosen as the optimum airflow rate for our DCDBD reactor and was used throughout experimental procedures.

Moreover, Fig. 5 (d) shows that at all sampling times, the degradation efficiency of SMX increases with an increased applied voltage, though complete removal of SMX was achieved after 60 min of the plasma experiment. So, after 50 min of plasma run, the highest SMX removal (97.72 %) was attained with 10 kV, compared to 97.75 and 96.86% obtained with 8 and 6.8 kV correspondingly. These observations suggest that higher voltage abundantly produces electrons around the inner and outer tubes of the DCDBD reactor whose energy is greater than the activation energy of chemical species such as O_2 and N_2 (Nifuku et al., 1997). This, therefore, leads to their effective fragmentation to diverse reactive entities in the air gap that is later circulated into the bulk solution where remediation of SMX pollutant occurred (Cheng et al., 2007, Nifuku et al., 1997). This agrees with Yan et al. (2006) and Cheng et al. (2007) who claimed that O_3 and OH^{\bullet} radicals are the major and most abundant oxidants in aqueous plasma environments. Their electrophilic attack on SMX followed by bond cleavage at higher applied voltages certainly led to enhanced decomposition. This trend was also reported in Bian et al. (2009) and Chen et al. (2015) during the decomposition of phenols by different pulse non-thermal plasma systems. Although a greater degradation percentage of SMX was reached with 10 kV, 8kV was selected as the optimum applied voltage due to plasma stability and to avoid sparking in the DCDBD system, and hence was used during the optimisation process.

3.4. Optimum conditions with DCDBD alone

Fig. 5 (e) shows the degradation of SMX at optimum conditions including SMX concentration 40 mg/L, initial pH 6.5, airflow rate 3 L/min, and peak voltage 8 kV. This validates that SMX was susceptible to O_3 attack and less exposed to OH^{\bullet} attack in plasma acidic environment. The degradation by-products of SMX identified after 30 min reaction time by LC-MS are listed in Table ST3 (supplementary material). The degradation of SMX pollutant ($C_{10}H_{12}N_3O_3S^+$, $m/z = 254.3$) after 30 min of DCDBD experiment at corresponding parameters resulted in six degradation intermediate by-products principally $C_9H_{14}NO_6S^+$, $C_8H_{12}NO_7S^+$, $C_6H_{10}NO_4S^+$, $C_7H_9N_3O_3S$, $C_6H_9NO_5S$ and $C_4H_7N_2O_3S^+$ corresponding to molecular mass of $m/z = 264.27, 163.17, 192.21, 215.23, 207.20,$ and 266.24 and elution times of 1.92, 1.47, 2.24, 0.42, 1.80, 1.72 min, separately.

The decomposition of SMX following the electrophilic attack of ozone augmented by hydroxyl radical interaction revealed the formation of six intermediates upon analysis. These outcomes also indicate that O_3 was abundantly produced in the DCDBD system and was more selective to SMX degradation than other reactive species (Massima Mouele et al., 2020). The functional groups $-NH_2$ and $-NH-$ in

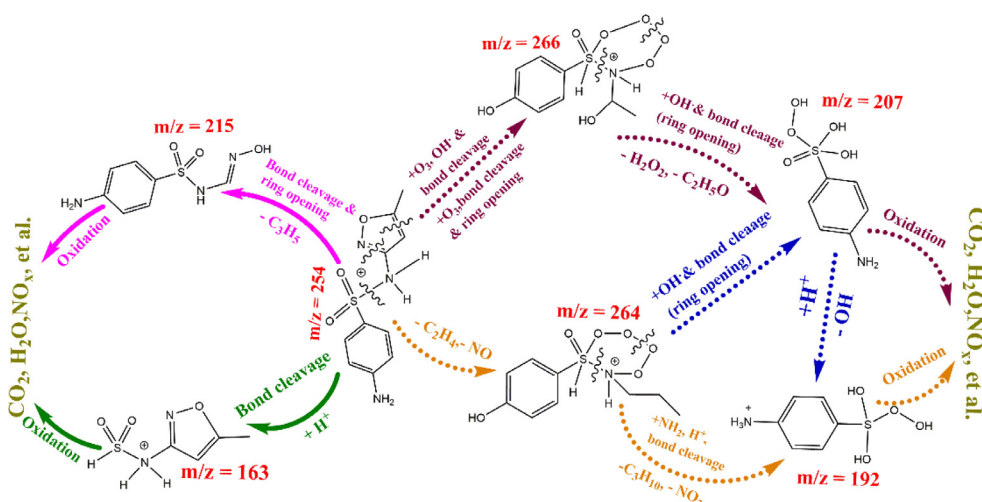


Fig. 6. Suggested degradation mechanism pathways of SMX decomposed by the DCDBD reactor at optimum conditions after 30 min reaction time: Applied voltage 8 kV, SMX concentration 40 mg/L, solution volume 1500 mL, solution pH 6.5, airflow rate 3 L/min, 1.5 mm silver electrode, 50 g/L NaCl inner electrode-electrolyte, air gap 2 mm and a plasma exposure time of 60 min.

the SMX carbon framework certainly served as bases and consequently boosted its degradation within 30 min of DCDBD treatment time. The suggested degradation pathways of SMX drug achieved with DCDBD alone are shown in Fig. 6.

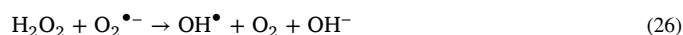
These results indicate that mineralisation of SMX reached above 30 min reaction time was typically initiated by bond or ring cleavage mechanisms on the protonated amide group and the heterocyclic five-membered ring in SMX chemical skeleton. This was seconded by the elimination of $-C_2H_4$, $-NO$, and $-C_3H_5$ that led to the formation of compounds with fragmentation pattern $m/z = 266$, 264 , 163 , and 215 , correspondingly as shown in Fig. 6. The metabolites formed showed that the mineralisation of SMX ($C_{10}H_{12}N_3O_3S^+$, $m/z = 254$) followed different paths unlike the report of Qi et al. (2014). The fragmentation of SMX in DCDBD alone was primarily initiated by nucleophilic addition of OH^\bullet , bond cleavage, and ring-opening by the elimination of $-H_2O_2$ and $-C_2H_5O$ that resulted in the formation of $m/z = 207$ that further mineralised to aqueous CO_2 , H_2O , and other inorganics.

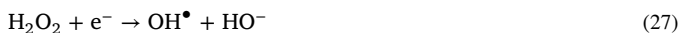
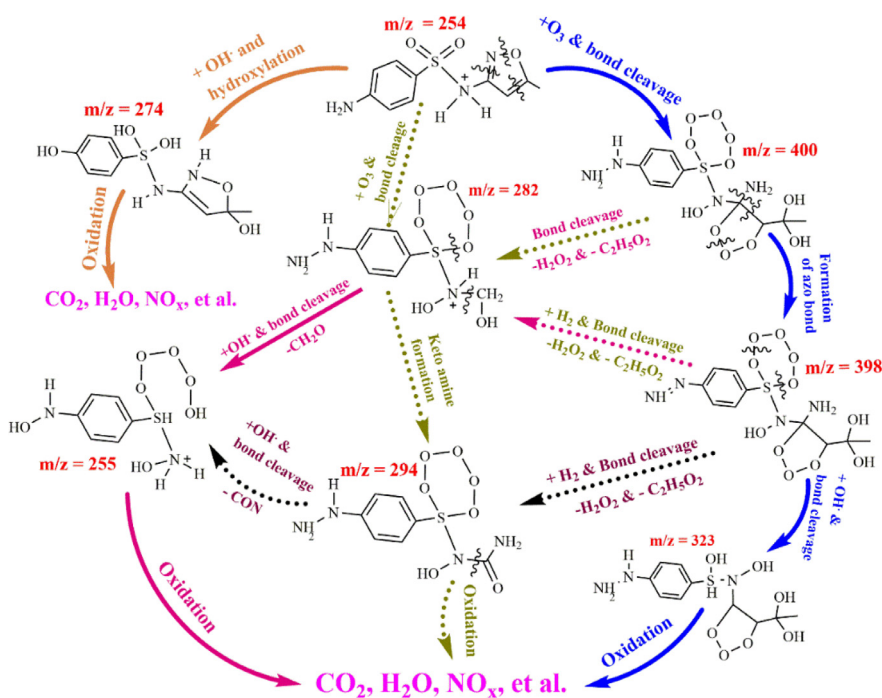
The bonding of $-NH_2$ group on $m/z = 264$ and its protonation seconded by ring cleavage and removal of $-C_3H_{10}$ and $-NO_2$ led to the formation of $m/z = 192$ that further oxidised and mineralised into CO_2 , H_2O , and simpler units. The last mechanistic pathways involved the oxidation of the degradation intermediates $m/z = 163$ and $m/z = 215$ directly into CO_2 , H_2O , and aqueous residues. This finding agrees with previous work reported by Kim et al. (2015) who established the decomposition mechanisms of sulfonamide antibiotics including SMX in a single cylindrical dielectric barrier discharge plasma actuator using air and oxygen as feed gases at diverse conditions. Their results showed that the absorption peak corresponding to SMX progressively declined with an increase of pH, signifying that SMX was degraded and mineralised into numerous inorganic entities such as SO_4^{2-} , NH_4^+ and NO_3^- . Nevertheless, the degradation efficiencies of model antibiotics and SMX in both air and oxygen ranged between 66.9 to 86.4%. In comparison with this study, the upsurge of pH noticed in their investigation indicated that O_3 likely dissociated into OH radicals that favoured the decomposition of SMX and related contaminants (qiong Gao et al., 2012). This study demonstrates that the DCDBD system is more efficient than the single cylindrical DBD developed by Kim et al. (2015) because, in our work, complete decomposition of SMX was achieved after 30 min of DCDBD run whereas the 86.4 % SMX removal was reached by Kim et al. (2015) after 60 min necessitated extended treatment time to reach completion. Even though noticeable removal percentages in consort with decomposition mechanism pathways of SMX using single or combined AOPs mainly ozonation, UV/visible light, ultrasound/ozone, etc. have been reported (Dantas et al., 2008, Trovó et al., 2009, Guo et al., 2015), the results obtained in the current research are more efficient and therefore authenticate that DCDBD is an effective advanced oxidation method

that can be used not only for complete oxidation and mineralisation of persistent pharmaceutical pollutants but for numerous toxins from contaminated water and wastewater sources. In addition, we attempted to prove that the efficacy of DCDBD reactor alone on SMX removal could be enhanced by examining the depollution behaviour of the targeted contaminant using DCDBD in combination with supported Ti/C-N-TiO₂ Nano catalyst.

3.5. Degradation of sulfamethoxazole by Ti/C-N-TiO₂ composites in the optimised DCDBD plasma configuration

Following the same procedure performed with DCDBD alone, sulfamethoxazole pharmaceutical model drug (SMX) was also subjected to the optimised DCDBD system combined with Ti/C-N-TiO₂ catalyst, and the results of the experiments were plotted in Fig. 5(e) Fig. 5.(e) indicates that the degradation of SMX with both DCDBD alone and DCDBD + Ti/C-N-TiO₂ followed a first-order reaction at corresponding rates of 3.79×10^{-2} ($R^2 = 0.999$) and $2.18 \times 10^{-2} \text{ min}^{-1}$ ($R^2 = 0.997$). Higher removal of SMX was achieved with DCDBD alone when compared with DCDBD + Ti/C-N-TiO₂ system. The superiority of DCDBD alone over DCDBD + Ti/C-N-TiO₂ could be ascribed to the production of OH^\bullet and co-species in DCDBD according to Equations (6 – 21) and their reaction on SMX pollutant. In contrast, the activation of the C-N-TiO₂ catalyst by the UV radiation generated in the DCDBD reactor is induced by both oxidation and reduction processes as previously described in Mouele et al. (2021). First, the penetration of UV light onto the C-N-TiO₂ surface promoted electrons (e^-) from the valence band (VB) of the catalyst to their excited state/conduction band (CB) leaving behind positively charged holes (h^+) on the VB (Eq. 22). The highly energised e^- reduces O_2 molecules to superoxide anions which by subsequent reactions produce OH^\bullet (Eqs. 23 – 27). On the other hand, the empty and positively charged h^+ oxidise water molecules to OH radicals following Eq. 28. Similar photocatalytic mechanistic steps for the generation of OH^\bullet were also outlined in Abdullah et al. (2016) during the degradation and mineralisation of phenol by hydrothermal synthesised C-N-TiO₂ catalyst under UV illumination.





These mechanisms coupled to those induced by the DCDBD alone make DCDBD + Ti/C-N-TiO₂ system adequate technology for pollution control. However, Fig. 5(e) shows that after 60 min of the experimental run, total removal of SMX (99.9%) was achieved with DCDBD alone compared to 86 % reached with DCDBD + Ti/C-N-TiO₂. This implies that SMX was recalcitrant in DCDBD + Ti/C-N-TiO₂ system due to the overshadowing of UV radiations by the Ti/C-N-TiO₂ catalyst mesh that was suspended around the inner tube of the DCDBD reactor (Fig.1), and consequently prevented effective diffusion of UV light produced by the plasma from interacting with the target pollutants. This also suggested that the water molecules and related species were not effectively cleaved off by UV light, this in return diminished the production of OH[•] and related oxidants that were supposed to enhance the detoxification of simulated SMX solution (Zhang et al., 2017). Consequently, the SMX degradation rate $5.7 \times 10^{-2} \text{ min}^{-1}$ ($R^2 = 0.999$) was obtained using DCDBD alone after 60 min decreased to $2.18 \times 10^{-2} \text{ min}^{-1}$ ($R^2 = 0.997$) by combining the photocatalyst composite in the DCDBD system.

This seems contradictory to the outcome of Chen et al. (2015) who investigated the removal of 17 β -estradiol (E2) by dielectric barrier discharge combined with powder Pt-TiO₂ catalyst and showed that 72.0% E2 removal was achieved with DBD alone compared to 98.9% reached with DBD combined with TiO₂ in acidic environment (pH 5.6). Their work shows that UV radiations generated in DBD systems play a crucial role in the production of free radicals that strengthen the detoxification of the targeted pollutant, but the decline of UV illumination in DBD systems may decrease its efficiency leading to reduced performance and hence lower degradation rate. Nevertheless, the results achieved in our study are promising because coating of the C-N-TiO₂ on Ti support is beneficial to avoid the post separation costs encountered with powder catalysts (Mouele et al., 2020). Beyond these aspects, the degradation of SMX by DCDBD + Ti/C-N-TiO₂ was also followed by examining the nature and intermediate by-products in DCDBD + Ti/C-N-TiO₂ systems using LC-MS, and the molecular and structural formula of the detected by-products are shown in Table ST4 (supplementary material) and their suggested degradation mechanism pathways in Fig. 7.

Fig. 7. Suggested degradation mechanism pathways of SMX decomposed by Ti/C-N-TiO₂ films hanged around the tube of DCDBD system at optimum conditions: Applied voltage 8 kV, SMX concentration 40 mg/L, solution volume 1.5 L, solution pH 6.5, airflow rate 3 L/min, 1.5 mm silver electrode, 50 g/L NaCl inner electrode-electrolyte, air gap 2 mm, (8 cm long x 2 cm large) x 4 coated films enfolded around the outer inner of the DCDBD reactor and a plasma running time of 60 min.

Table ST4 (supplementary material) displays SMX degradation intermediate by-products obtained with DCDBD + Ti/C-N-TiO₂ and their IUPAC nomenclature. The tabulated data indicate that SMX (C₁₀H₁₂N₃O₃S⁺, m/z = 254.3) was fragmented into seven degradation intermediate metabolites C₇H₁₀N₄O₇S (m/z = 294.2), C₁₀H₁₆N₄O₁₁S (m/z = 400.3), C₇H₁₂N₃O₇S⁺ (m/z = 282.2), C₁₀H₁₄N₄O₁₁S (m/z = 398.3), C₆H₁₁N₂O₇S⁺ (m/z = 255.2), C₁₀H₁₇N₃O₇S (m/z = 323.3) and C₁₀H₁₄N₂O₅S (m/z = 274.3) that eluted after 6.54, 10.99, 11.33, 10.69, 8.48, 7.76 and 6.34 min, respectively. These fragmentation by-products have not been outlined elsewhere. The decay mechanism in Fig. 7 shows that the degradation of SMX occurred via four different pathways. The hydroxylation of SMX resulted in m/z = 274 metabolite that was mineralised into aqueous liquified CO₂, H₂O, and inorganic salts (Guo et al., 2015, Dirany et al., 2010). On the other hand, the interaction of O₃ with SMX which followed bond cleavage yielded compound m/z = 282 epoxide which interacted with OH radicals based on bond cleavage mechanism and yielded m/z = 255 that further transformed to CO₂, H₂O, and harmless inorganics. The bond cleavage of the m/z = 282 intermediate led to the formation of m/z = 294 keto amine that was mineralised into H₂O, dissolved CO₂, and related metabolites. The fourth pathway involved hydroxylation and bond cleavage reaction of SMX that yielded m/z = 400 which by substitution and rearrangement resulted in m/z = 398 intermediate. This later reacted with OH[•] and transformed into m/z = 323 that was further mineralised to CO₂, H₂O, NO_x, and other harmless end-products. In comparison with DCDBD alone, the removal of SMX with DCDBD + Ti/C-N-TiO₂ led to seven intermediate by-products whose slow oxidation possibly sustains the resistant behaviour of the fragmentation by-products that hindered the complete mineralisation of SMX, requiring prolonged treatment time and lower rate (Guo et al., 2015, Dirany et al., 2010). Conversely, the complete degradation of SMX achieved with DCDBD alone after 30 min resulted in only six degradation metabolites that were rapidly mineralised (Fig. 7). The 86 % efficiency of the C-N-TiO₂ catalyst immobilised on Ti support demonstrates the effectiveness of the DCDBD/Ti/C-N-TiO₂ system and could be ascribed to morphological defects of Ti/C-N-TiO₂ film that happened after the dip-coating of C-N-TiO₂ nano catalyst on pure Ti mesh substrate (Fig. 2 (a & b)). Thus, the method of coating

catalyst on the substrate and the choice of the catalytic support are vital features in film engineering and hence should be adjusted carefully to develop photocatalytic films with favourable attributes. The mesh size of the support could also be enlarged to minimize shadowing of UV emissions, but this would lower the amount of active catalyst surface area too.

3.5.1. Kinetics study and comparison with literature

Non-thermal plasma (NTP) technologies have been widely used for the remediation of water and wastewater (Mouele et al., 2015, Magureanu et al., 2021), however, the efficiency of their configurations varies from one technology to another depending on various factors including the type of plasma reactor, nature of the targeted chemical, and the recalcitrance of their metabolites and degradation intermediate by-products (Massima Mouele et al., 2021). Consequently, previous investigations suggested that the energy yield (G_{50}) required for the conversion of 50 % of targeted pollutants can be used as a convenient factor to compare the efficiency of NTP reactors employed in water and wastewater treatment (Magureanu et al., 2013, Grabowski et al., 2007). Yet, the value of G_{50} may depend on various parameters including pollutant initial concentration, solution volume, input/dissipated power (w), degradation efficiency (D%), treatment time (t, min), rate constant (Kr, min^{-1}), and half-life ($T_{1/2}$, min). Depending on the type of feed gas used, Grabowski et al. (2007) outlined that the performance of a typical DBD system operated under dry air flow could be 400 times higher than that of the reference reactor. This complements the report of Malik (Malik, 2010). This may upsurge to 2000 times higher than the reference reactor when oxygen is used as feed gas (Nakagawa et al., 2003). Similarly, the electrical efficiency per order (EE/O) expressed in $\text{kWh/m}^3 \text{ order}^{-1}$ as described in Eq. (29) is another useful parameter reported by Asaithambi et al. (2015) to define comparative efficiency of advanced oxidation processes (AOPs). Therefore, the EE/O was used in this study to complement G_{50} in comparison of effectiveness of the current DCDBD reactor with those explored in previous studies.

$$EE/O = \frac{38.4 \times PeI}{V \times k} \quad (29)$$

Where P_{el} is the electrical power input (kW), t is the plasma treatment time (min), V is the volume (L) of SMX, k (min^{-1}) is the pseudo-first-order rate constant for the degradation of SMX pollutant.

Asaithambi et al. (2015) claimed that most effective treatment system correspond to lower energy consumption, however, this may diverge depending on the applied experimental conditions. In our study, the estimated energy efficiency G_{50} of the DCDBD reactor alone and DCDBD/Ti/C-N-TiO₂ operated under 3L/min air flow used for the degradation of 50 % SMX as well as the electrical efficiency per order (EE/O) of DCDBD alone and DCDBD/Ti/C-N-TiO₂ at the optimum conditions was compared with previous studies and are shown in Table 3. Data recorded in Table 3 show that higher values of G_{50} indicate better efficiency/performance of the NTP reactor which are also characterised by lower values of EE/O. For example, in the report of Magureanu et al. (2013), the full degradation of 300 mL of 50 mg/L of three pharmaceutical residues diketopiperazine, enalapril, and enalaprilat, in a co-axial DBD reactor at the same power of 2 W was achieved after 120, 90, and 30 min, respectively. The degradation of 50 % of the three pollutants required 87, 9 and 3 min corresponding to the energy yields of 43.21, 412.62 and 1245.526 g/kWh, and the EE/O of 1.113, 3.368 and 32 $\text{kWh/m}^3 \text{ order}^{-1}$, respectively. This implied that their co-axial DBD configuration was more effective for the removal of Enalaprilat followed by Enalapril and Diketopiperazine. In our investigation, the energy yield G_{50} required for the degradation of 50 % of 1500 mL 40 mg/L SMX with DCDBD alone at a power of 60 W reached 34.64 g/kWh at an EE/O of 40.527 $\text{kWh/m}^3 \text{ order}^{-1}$ within 18 min though its total mineralisation was achieved after 30 minutes of DCDBD run. On the other hand, the decomposition of 50% SMX with DCDBD/Ti/C-N-TiO₂ system at the same concentration, volume, and power, was achieved within 32 min and corresponded to an energy yield of 19.787 g/kWh and an EE/O

of 70.458 $\text{kWh/m}^3 \text{ order}^{-1}$ though pollutant complete removal required prolonged treatment time. These energy yields and electrical efficiency per order indicate that both systems are effective in the removal of SMX contaminant, however the twofold decline of the G_{50} and increase of EE/O values of SMX degradation was attributed to the shadowing of the UV light by the supported catalyst. This certainly limited the production of active oxidants mainly O₃ and OH[•] in the solution, which consequently decelerated the rate of conversion of SMX from 0.0379 min^{-1} with DCDBD alone to 0.0218 min^{-1} with DCDBD/Ti/C-N-TiO₂. The change in time for full mineralisation of SMX from 30 min to more than 60 min recorded with DCDBD alone and DCDBD/Ti/C-N-TiO₂, respectively is also due to the recalcitrance of the abundant degradation intermediate by-products early schemed in Figs. 6 and 7.

Comparing literature in Table 3 with the actual study, the energy yields G_{50} 1786.96 and 544.19 g/kWh corresponding to EE/O of 2.10 and 5.120 $\text{kWh/m}^3 \text{ order}^{-1}$ reported by (Hu and Wang, 2021) and (Magureanu et al., 2010), for the degradation of 50 % of pefloxacin (PEF) and pentoxifiline (PXF), respectively appear higher than 19.747 and 34.64 g/kWh achieved at 40.527 and 70.458 $\text{kWh/m}^3 \text{ order}^{-1}$ in our study. This could be ascribed to the small volumes 100 and 200 mL of the PEF and PXF pollutants used, which are 15 and 7 times smaller than 1500 mL of SMX used in the current DCDBD reactor. Next, the structural resistant behaviour of PEF, PXF, and their degradation intermediate by-products were vulnerable in DBD acidic media dictated by their half-lives 5 and 15 min at rate constants of 0.13 and 0.045 min^{-1} , correspondingly; as compared to SMX and its amides and amines intermediate metabolites being resistant in aqueous DCDBD media complemented by their slightly elevated half-lives of 18.34 and 32 min with low-rate constants of 0.0379 and 0.0218 min^{-1} , respectively.

A similar trend is observed in the study conducted by Magureanu et al. (2013) previously highlighted during degradation of enalapril and its metabolite enalaprilat with corresponding G_{50} 412.62 and 1245.526 g/kWh and EEO of 3.368 and 32 $\text{kWh/m}^3 \text{ order}^{-1}$ were reached at lower volume of 300 mL and half-lives of 9.1 and 3 min, respectively. The G_{50} 412.62 and 1245.526 g/kWh are higher than those obtained in the current study and their corresponding EE/O of 3.368 and 32 $\text{kWh/m}^3 \text{ order}^{-1}$ are inversely lower than our electrical efficiency per order 40.527 and 70.458 $\text{kWh/m}^3 \text{ order}^{-1}$. This can be argued as the amount of pollutant 1500 mL treated in the DCDBD is four times higher than 300 mL used in their study. These discrepancies are also due to the different nature of SMX from that of enalapril, its metabolite enalaprilat, and diketopiperazine whose degradation intermediate by-products required short and prolonged treatment times at varied rates constants. Though their co-axial DBD system seems effective for the degradation of diketopiperazine degradation intermediate by-product with a G_{50} of 43.21 g/kWh and a lower EE/O of 1.113 $\text{kWh/m}^3 \text{ order}^{-1}$, its half-life 87 min shows that diketopiperazine was recalcitrant than parent molecules. Apart from lower solution volumes utilised in Magureanu et al. (2013), the complete mineralisation of enalapril and its metabolites required extended treatment time between 30 -120 min as compared to 30 – 60 min required for total oxidation of SMX in our study. This indicates that DCDBD reactor in Fig. 1 is adequately performant for the removal of pharmaceutical recalcitrant residues in water and wastewater treatment facilities. In addition, the abatement of 200 mL of 0.249 mol/L oxacillin carried out by Magureanu et al. (2011) in DBD with falling liquid configuration yielded a G_{50} of 3815.174 g/kWh at a very low EE/O of 1.002 $\text{kWh/m}^3 \text{ order}^{-1}$ with a half-life of 1.31 min. This implies that oxacillin and its degradation intermediate by-products were weak in DBD oxidative environment though their complete removal was achieved after 30 min of DBD run. Since the 200 mL oxacillin is 7 times smaller than 1500 mL SMX used in the current study and the half-life 1.31 min recorded in Table 3 is shorter than 18.3 or 32 min, this sustains the superior effectiveness of the DCDBD reactor optimised in our study. Nevertheless, both DCDBD and DCDBD /Ti/C-N-TiO₂ systems appear effective for the degradation of SMX pharmaceutical

Table 3Comparison of the energy yield G_{50} required to decompose 50% of pharmaceutical contaminants by non-thermal plasma advanced technologies with that of DCDBD reactor

Pollutant	C_0 (mol/L)	Molecular weight (g/mol)	Volume (mL)	Degradation system	P (kW)	D %	Treatment time (min)	Kr (min^{-1})	$t_{1/2}$ (min)	G_{50} (g/kWh)	EE/O (kWh/m^3 order ¹)	References
Norfloracin (NOR)	0.031	319.331	10	DBD/ H_2O_2 (0.5mmol/L) / Fe^{2+}	0.060	98	0.5	7.82	0.10	8.249	29.463	(Xu et al., 2020)
Glucocorticoids (GCs)	0.055	360.4	300	Peroxymonosulfate, microbubble/DBD	0.0835	61-82	90	0.010 – 0.019	6.93 -36.47	5.138 – 0.976	1068.80 - 562.26	(Miruka et al., 2021)
Pefloxacin (PEF)	0.4	333.358	100	DBD	0.0007	96.10	25	0.13	5.33	1786.96	2.10	(Hu and Wang, 2021)
Veterinary antibiotics	0.020	236.269	1000	Single cylindrical DBD	0.0089	90	30	0.073	9.5	27.94	4.680	(Kim et al., 2013)
Carbamazepine	0.189	136.269	1000	DBD rotating reactor	0.75	94	60	0.0468	14.81	1.159	615.384	(Kim et al., 2015)
Amoxicillin	0.1368	365.4	1000	DBD rotating reactor	0.75	99.99	10	0.332	2.08	16.021	86.750	(Kim et al., 2015)
Pentoxifiline (PXF)	0.359	278.31	200	DBD	0.0012	92.5	60	0.045	15.3	544.19	5.120	(Magureanu et al., 2010)
Diketopiperazine	0.140	358	300	Co-axial DBD	0.002	62	120	0.008	87	43.21	32	(Magureanu et al., 2013)
Enalapril	0.133	376.4267	300	Co-axial DBD	0.002	99.99	90	0.076	9.1	412.62	3.368	(Magureanu et al., 2013)
Enalaprilat	0.143	348.399	300	Co-axial DBD	0.002	99.99	30	0.230	3	1245.526	1.113	(Magureanu et al., 2013)
Oxacillin	0.249	401.436	200	DBD with falling liquid	0.002	99.99	30	0.383	1.31	3815.174	1.002	(Magureanu et al., 2011)
Phenol	0.10	94.11	1000	DBD	0.50	99.99	60	0.115	6.02	1.563	166.956	(Krause et al., 2011)
Clofibrin acid	0.10	214.645	1000	DBD	0.50	99.99	30	0.230	3.0	7.154	83.478	(Krause et al., 2011)
Iopromide	0.10	791.11	1000	DBD	0.75	98	60	0.065	10.66	4.95	443.10	(Krause et al., 2011)
Carbamazepine	0.10	236.269	1000	DBD	0.75	94	60	0.047	14.74	0.178	612.766	(Krause et al., 2011)
Carbamazepine	0.379	236.269	200	Ex situ DBD system	0.012	90	60	0.038	18.23	4.55	60.632	(Magureanu et al., 2011)
Aniline	0.107	93.13	300	DBD/micro bubbles	0.0382	82.7	60	0.029	23.73	3.30	168.610	(Liu et al., 2019)
Phenol	0.010	94.11	70	DBD	0.0026	99.99	30	0.150	4.62	3.01	9.51	(Ceriani et al., 2018)
Hydrochlorothiazide	0.010	358	70	DBD	0.0026	99.99	30	0.10	6.93	6.95	32.914	(Ceriani et al., 2018)
Paracetamol	0.066	151.163	1500	DBD	0.50	99.99	30	0.23	3	1.50	55.652	(yi Pan and chen Qiao, 2019)
Aniline	1.073	93.13	10	DBD	0.0173	90.2	12	0.194	3.57	0.062	342.433	(Sang et al., 2019)
Chlorobenzen	1.770	112.56	50	Corona discharge	0.092	99.99	12	0.177	3.91	13.846	399.186	(Jose and Philip, 2019)
Diclofenac (DCF)	0.168	296.148	55	Corona discharge	0.024	99.99	15	0.046	15	15.20	364.300	(Dobrin et al., 2013)
Sulfadiazine antibiotics	0.039	250.278	100	Water falling film DBD	0.15	87	30	0.068	10.19	0.319	847.058	(Rong et al., 2014)
1,7- α -ethinylestradiol (EE2)	0.00337	296.4	60	Single cylindrical DBD	0.0397	99.8	20	0.31	3.10	0.243	819.612	(Wardenier et al., 2019)
Carbamazepine and 1,7- α ethinylestradiol	0.0039 – 0.00337	236.269 & 296.4	500	Single cylindrical DBD	0.04 – 0.09	90 – 99.5	30	0.073 – 0.176	13.19–5.47	0.44 – 0.452	42.082 – 39.272	(Wardenier et al., 2018)
Diclofenac	0.337	296.148	100	Double cylindrical DBD	0.050	99.9	10	0.921	1.04	1.992	20.850	(Rong et al., 2014)
Sulfamethoxazole (MX)	0.20	236.269	1500	DBD alone	0.060	99.99	30	0.0379	18.28	34.640	40.527	This study
Sulfamethoxazole (MX)	0.20	253.279	1500	DBD + Ti/C-N- TiO_2	0.060	86.4	60	0.0218	32	19.787	70.458	This study

residue as compared to previous reports shown in Table 3. In addition, data outlined in Table 3 showed that the energy yield (G_{50}) for the degradation of various pharmaceutical water contaminants (with concentration range of 0.00337 – 1.779 mol/L and volume range of 10–1000 mL) using various NTP configurations resulted in the range of 0.062 to 3815.174 g/kWh at corresponding EE/O of 342.433 – 1.002 kWh/m³ order¹ (Krause et al., 2011, Magureanu et al., 2011, Liu et al., 2019, Ceriani et al., 2018, yi Pan and chen Qiao, 2019, Sang et al., 2019, Jose and Philip, 2019, Dobrin et al., 2013, Rong et al., 2014, Wardenier et al., 2019, Wardenier et al., 2018, Rong et al., 2014); which appear below the values achieved with DCDBD alone and DCDBD/Ti/C-N-TiO₂ system during removal of SMX. These confirm that the DCDBD actuator in Fig. 1 is highly performant, though pollutant initial concentrations and solution volumes, power, half-lives, rate constants and times required for their complete removal differ from one another. These trends show that NTP configurations, mainly DBD reactors are effective advanced treatment processes for the remediation of pharmaceutical contaminants from water and wastewater. The DCDBD investigated in our study is a promising advanced treatment method for pharmaceuticals remediation that can be used solely or in combination with photocatalysts as a point of use advanced technology in water and wastewater treatment facilities. The novelty of this work mostly highlighted by the energy yield G_{50} (g/kWh) and electrical efficiency per order (EE/O) shows that both DCDBD and DCDBD/Ti/C-N-TiO₂ systems are effective treatment methods for the removal of pharmaceutical contaminants from water and wastewater effluents as compared to previous reports. The C-N-TiO₂ nano catalyst is successfully adherent on Ti mesh being proved suitable catalytic support. The prepared Ti/C-N-TiO₂ films exhibit impeccable antibacterial properties and are photo catalytically active. These findings have not been published elsewhere.

4. Conclusions and prospects

In a previous report (Mouele et al., 2020), we proved that the powder C-N-TiO₂ Nanocatalyst was effective for the removal of organic pollutants such as O.II dye, however, the post-separation of the catalyst from the treated effluent could be challenging at the industrial level, costly and time-consuming.

In addition, TiO₂ catalysts have previously been immobilised on SS mesh however, corrosion of SS support was experienced and needed to be overcome (Tijani et al., 2017, Tijani et al., 2017). This study demonstrates that Ti is excellent catalytic support and proved that C-N-TiO₂ was adherent on Ti mesh.

Therefore, supporting the catalyst on pure Ti mesh could be an alternative to employ C-N-TiO₂ Nanocatalyst combined with the DCDBD system, hence forming a dual advanced oxidation process that can utilise the UV generated by the DCDBD system to reach desirable outcomes.

Herein, we successfully optimised the DCDBD reactor by assessing the impact of various factors such as initial concentration, solution pH, air flow rate, and the applied voltage on the degradation percentages of the SMX drug. The optimum concentration of 40 mg/L was quickly degraded at a pH of 6.5, airflow rate of 3 L/min at the applied voltage of 8 kV.

Complete degradation of SMX with the optimised DCDBD alone was achieved within 30 min. The decomposition of SMX yielded six degradation by-products whose mineralisation was achieved at a rate of $1.027 \times 10^{-1} \text{ min}^{-1}$. The energy yield G_{50} required to degrade 50 % of SMX pollutant reached 34.64 g/kWh with a corresponding and electrical efficiency per order (EE/O) of 40.527 kWh/m³ order¹ with DCDBD alone within 18 min showing excellent performance of the DCDBD configuration as compared to literature.

The nanocatalyst C-N-TiO₂ was successfully deposited on pure Ti mesh (Ti/C-N-TiO₂) by a sol-gel and dip coating processes followed by pyrolysis. SEM analysis showed that Ti/C-N-TiO₂ films had different morphologies. That is, the porous C-N-TiO₂ nanocrystals were formed

as fine particles and completely covered pure Ti mesh. Although Ti/C-N-TiO₂ films showed excellent antibacterial activity, their incorporation in the plasma reactor was effective but prolonged the complete mineralisation of SMX to more than 60 min due to the shadowing of the UV light produced by the plasma in the DCDBD reactor and hence reduced the photocatalytic degradation efficiencies of the pollutant.

Total degradation of SMX with the DCDBD/ Ti/C-N-TiO₂ combined system was nearly attained after 60 min of plasma run and resulted in the formation of seven intermediate by-products that were gradually mineralised at a rate of $2.18 \times 10^{-2} \text{ min}^{-1}$. The degradation of 50 % SMX with DCDBD/ Ti/C-N-TiO₂ system corresponded to an energy yield of 19.787 g/kWh achieved with an electrical efficiency per order (EE/O) of 70.458 kWh/m³ order¹ after 32 min. Both systems optimised DCDBD alone and DCDBD/Ti/C-N-TiO₂ systems show great performance toward the removal of pharmaceutical water toxins as compared to previous studies.

In this study, the optimised DCDBD reactor was demonstrated effective for the degradation of the selected contaminant. The integration of the photocatalyst supported on Ti mesh provides a proof of concept for combined advanced remediation technologies. However, the choice of the support and immobilisation technique is critical to achieving maximum depollution.

For future investigations, the catalysts should directly be immobilised on the inner dielectric tube of the DCDBD reactor. This would be another route to use the maximum of the UV radiation generated in the optimised DCDBD reactor and hence to reach excellent pollution control in shorter times.

Funding

The authors are appreciative of Water Research Commission (WRC) SA for funding this work through Core Project 18N/2019.

Declaration of Competing Interest

The authors declare that there is no conflict of interest in publishing this manuscript.

CRediT authorship contribution statement

Emile Salomon Massima Mouele: Writing – original draft, Writing – review & editing. **Tay Zar Myint Myo:** Writing – original draft, Writing – review & editing. **Htet Htet Kyaw:** Writing – original draft, Writing – review & editing. **Jimoh O Tijani:** Writing – original draft, Writing – review & editing. **Mihaela Dinu:** Writing – original draft, Writing – review & editing. **Anca C Parau:** Writing – original draft, Writing – review & editing. **Iulian Pana:** Writing – original draft, Writing – review & editing. **Youssef El Ouardi:** Writing – original draft, Writing – review & editing. **Jamal Al-Sabahi:** Writing – original draft, Writing – review & editing. **Mohammed Al-Belushi:** Writing – original draft, Writing – review & editing. **Eduard Sosnin:** Writing – original draft, Writing – review & editing. **Victor Tarasenko:** Writing – original draft, Writing – review & editing. **Cheng Zhang:** Writing – original draft, Writing – review & editing. **Tao Shao:** Writing – original draft, Writing – review & editing. **Tanta Verona Iordache:** Writing – original draft, Writing – review & editing. **Sandu Teodor:** Writing – original draft, Writing – review & editing. **Katri Laatikainen:** Writing – original draft, Writing – review & editing. **Alina Vladescu:** Writing – original draft, Writing – review & editing. **Mohammed Al-Abri:** Supervision, Writing – original draft, Writing – review & editing. **Andrei Sarbu:** Writing – original draft, Writing – review & editing. **Mariana Braic:** Writing – original draft, Writing – review & editing. **Viorel Braic:** Writing – original draft, Writing – review & editing. **Sergey Dobretsov:** Supervision, Writing – original draft, Writing – review & editing. **Leslie F Petrik:** Supervision, Writing – original draft, Writing – review & editing.

Acknowledgments

The author acknowledges all funders of this project including WRC and NRF (SA), Environmental and Nano Science (ENS) research group for their financial assistance. A.V. thanks Tomsk Polytechnic University within the framework of the Tomsk Polytechnic University-Competitiveness Enhancement Program grant. The thanks are extended to all ENS internship students for their technical assistance. Thanks, are also addressed to all Co-authors from Oman and Romania, China and Russia, Nigeria and Finland who significantly contributed to the peer review of this manuscript.

Supplementary materials

Supplementary material associated with this article can be found, in the online version, at doi:10.1016/j.hazadv.2022.100051.

References

- Abdullah, A.M., Al-Thani, N.J., Tawbi, K., Al-Kandari, H., 2016. Carbon/nitrogen-doped TiO₂: New synthesis route, characterization and application for phenol degradation. *Arab. J. Chem.* 9, 229–237. doi:10.1016/j.arabjc.2015.04.027.
- Adeyuyi, Y.G., 2005. Sonochemistry in environmental remediation. 1. Combinative and hybrid sonophotocatalytic oxidation processes for the treatment of pollutants in water. *Environ. Sci. Technol.* 39, 3409–3420. doi:10.1021/es049138y.
- Asaithambi, P., Saravanathamizhan, R., Matheswaran, M., 2015. Comparison of treatment and energy efficiency of advanced oxidation processes for the distillery wastewater. *Int. J. Environ. Sci. Technol.* 12, 2213–2220. doi:10.1007/s13762-014-0589-9.
- Beltrán, F.J., Aguinaco, A., García-Araya, J.F., Orpessa, A., 2008. Ozone and photocatalytic processes to remove the antibiotic sulfamethoxazole from water. *Water Res* 42, 3799–3808. doi:10.1016/j.watres.2008.07.019.
- Bian, W., Ying, X., Shi, J., 2009. Enhanced degradation of p-chlorophenol in a novel pulsed high voltage discharge reactor. *J. Hazard. Mater.* 162, 906–912. doi:10.1016/j.jhazmat.2008.05.156.
- Çomaklı, O., Yetim, T., Çelik, A., 2014. The effect of calcination temperatures on wear properties of TiO₂ coated CP-Ti. *Surf. Coatings Technol.* 246, 34–39. doi:10.1016/j.surfcoat.2014.02.059.
- Çomaklı, O., Yazıcı, M., Yetim, T., Yetim, A.F., Çelik, A., 2016. The effect of calcination temperatures on structural and electrochemical properties of TiO₂ film deposited on commercial pure titanium. *Surf. Coatings Technol.* 285, 298–303. doi:10.1016/j.surfcoat.2015.11.055.
- Ceriani, E., Marotta, E., Shapoval, V., Favaro, G., Paradisi, C., 2018. Complete mineralization of organic pollutants in water by treatment with air non-thermal plasma. *Chem. Eng. J.* 337, 567–575. doi:10.1016/j.cej.2017.12.107.
- Chan, S.H.S., Wu, T.Y., Juan, J.C., Teh, C.Y., 2011. Recent developments of metal oxide semiconductors as photocatalysts in advanced oxidation processes (AOPs) for treatment of dye waste-water. *J. Chem. Technol. Biotechnol.* 86, 1130–1158. doi:10.1002/jctb.2636.
- Chen, Y., Sun, L., Yu, Z., Wang, L., Xiang, G., Wan, S., 2015. Synergistic degradation performance and mechanism of 17 β -estradiol by dielectric barrier discharge non-thermal plasma combined with Pt-TiO₂. *Sep. Purif. Technol.* 152, 46–54. doi:10.1016/j.seppur.2015.07.061.
- H.-H. Cheng, S.-S. Chen, Y. Wu, D. Ho, Non-thermal plasma technology for degradation of organic compounds in wastewater control: A critical review, Undefined. (2007).
- Dantas, R.F., Contreras, S., Sans, C., Esplugas, S., 2008. Sulfamethoxazole abatement by means of ozonation. *J. Hazard. Mater.* 150, 790–794. doi:10.1016/j.jhazmat.2007.05.034.
- de A.G.U. de Souza, S.M., Bonilla, K.A.S., de Souza, A.A.U., 2010. Removal of COD and color from hydrolyzed textile azo dye by combined ozonation and biological treatment. *J. Hazard. Mater.* 179, 35–42. doi:10.1016/j.jhazmat.2010.02.053.
- de O. Souza, H., dos S. Costa, R., Quadra, G.R., dos S. Fernandez, M.A., 2021. Pharmaceutical pollution and sustainable development goals: Going the right way? *Sustain. Chem. Pharm.* 21.
- Dhanke, P., Wagh, S., Kanse, N., 2018. Degradation of Fish Processing Industry Wastewater in Hydro-cavitation Reactor. *Mater. Today Proc.* 5, 3699–3703.
- Dimitrakopoulou, D., Rethemiotaki, I., Frontistis, Z., Xekoukoulakis, N.P., Venieri, D., Mantzavinos, D., 2012. Degradation, mineralization and antibiotic inactivation of amoxicillin by UV-A/TiO₂ photocatalysis. *J. Environ. Manage.* 98, 168–174. doi:10.1016/j.jenvman.2012.01.010.
- Dirany, A., Sirés, I., Oturan, N., Oturan, M.A., 2010. Electrochemical abatement of the antibiotic sulfamethoxazole from water. *Chemosphere* 81, 594–602. doi:10.1016/j.chemosphere.2010.08.032.
- Dobrin, D., Bradu, C., Magureanu, M., Mandache, N.B., Parvulescu, V.I., 2013. Degradation of diclofenac in water using a pulsed corona discharge. *Chem. Eng. J.* 234, 389–396. doi:10.1016/j.cej.2013.08.114.
- M. Erofeev, M. Lomaev, V. Ripenko, M. Shulepov, D. Sorokin, V. Tarasenko, Generators of Atmospheric Pressure Diffuse Discharge Plasma and Their Use for Surface Modification, *Plasma* 2 (2019) 27–38. doi:10.3390/plasma2010004.
- Erofeev, V.I., Dzhililova, S.N., Erofeev, M.V., Ripenko, V.S., Reschetilowski, V.P., 2020. Conversion of the propane-butane fraction into arenes on MFI zeolites modified by zinc oxide and activated by low-temperature plasma. *Molecules* 25. doi:10.3390/molecules25112704.
- Ghazzal, M.N., Wojcieszak, R., Raj, G., Gaigneaux, E.M., 2014. Study of mesoporous cds-quantum-dot-sensitized TiO₂ films by using x-ray photoelectron spectroscopy and afm. *Beilstein J. Nanotechnol.* 5, 68–76. doi:10.3762/bjnano.5.6.
- Glaze, W.H., 1986. Reaction Products of Ozone: A Review. *Environ. Health Perspect.* 69, 151–157.
- Gogate, P.R., Pandit, A.B., 2004. A review of imperative technologies for wastewater treatment I: oxidation technologies at ambient conditions. *Adv. Environ. Res.* 8, 501–551. doi:10.1016/S1093-0191(03)00032-7.
- Gogniat, G., Thyssen, M., Denis, M., Pulgarin, C., Dukan, S., 2006. The bactericidal effect of TiO₂ photocatalysis involves adsorption onto catalyst and the loss of membrane integrity. *FEMS Microbiol. Lett.* 258, 18–24. doi:10.1111/J.1574-6968.2006.00190.X.
- Grabowski, L.R., Van Veldhuizen, E.M., Pemen, A.J.M., Rutgers, W.R., 2007. Breakdown of methylene blue and methyl orange by pulsed corona discharge. *Plasma Sources Sci. Technol.* 16, 226–232. doi:10.1088/0963-0252/16/2/003.
- Guo, W.Q., Yin, R.L., Zhou, X.J., Du, J.S., Cao, H.O., Yang, S.S., Ren, N.Q., 2015. Sulfamethoxazole degradation by ultrasound/ozone oxidation process in water: Kinetics, mechanisms, and pathways. *Ultrason. Sonochem.* 22, 182–187. doi:10.1016/j.ultrasonch.2014.07.008.
- Gupta, V.K., Ali, I., Saini, V.K., 2007. Adsorption studies on the removal of Vertigo Blue 49 and Orange DNA13 from aqueous solutions using carbon slurry developed from a waste material. *J. Colloid Interface Sci.* 315, 87–93.
- He, D., Sun, Y., Xin, L., Feng, J., 2014. Aqueous tetracycline degradation by non-thermal plasma combined with nano-TiO₂. *Chem. Eng. J.* 258, 18–25. doi:10.1016/j.cej.2014.07.089.
- Heinlaan, M., Ivask, A., Blinova, I., Dubourguier, H.C., Kahru, A., 2008. Toxicity of nanosized and bulk ZnO, CuO and TiO₂ to bacteria *Vibrio fischeri* and crustaceans *Daphnia magna* and *Thamnocephalus balticus*. *Chemosphere* 71, 1308–1316. doi:10.1016/j.chemosphere.2007.11.047.
- Hu, X., Wang, B., 2021. Removal of pefloxacin from wastewater by dielectric barrier discharge plasma: Mechanism and degradation pathways. *J. Environ. Chem. Eng.* 9. doi:10.1016/j.jece.2021.105720.
- Ikehata, K., Jodeiri Naghashkar, N., Gamal El-Din, M., 2006. Degradation of aqueous pharmaceuticals by ozonation and advanced oxidation processes: A review. *Ozone Sci. Eng.* 28, 353–414. doi:10.1080/01919510600985937.
- M. Iqbal, A. Bhatti, I. Ahmad, Photo-degradation of the methyl blue: Optimization through response surface methodology using rotatable center composite design, 2013.
- Jiang, B., Zheng, J., Lu, X., Liu, Q., Wu, M., Yan, Z., Qiu, S., Xue, Q., Wei, Z., Xiao, H., Liu, M., 2013. Degradation of organic dye by pulsed discharge non-thermal plasma technology assisted with modified activated carbon fibers. *Chem. Eng. J.* 215–216, 969–978. doi:10.1016/j.cej.2012.11.046.
- Jose, J., Philip, L., 2019. Degradation of chlorobenzene in aqueous solution by pulsed power plasma: Mechanism and effect of operational parameters. *J. Environ. Chem. Eng.* 7. doi:10.1016/j.jece.2019.103476.
- K.M. Kalumuck, G.L. Chahine, The Use of Cavitating Jets to Oxidize Organic Compounds in Water, (2000).
- Karunakaran, C., Gomathisankar, P., Manikandan, G., 2010. Preparation and characterization of antimicrobial Ce-doped ZnO nanoparticles for photocatalytic detoxification of cyanide. *Mater. Chem. Phys.* 123, 585–594. doi:10.1016/j.materchemphys.2010.05.019.
- Kim, K.-S., Kim, H.Woo, 2003. Synthesis of ZnO nanorod on bare Si substrate using metal organic chemical vapor deposition. *Phys. B* 328, 368–371. doi:10.1016/S0921-4526(02)01954-3.
- Kim, K.S., Yang, C.S., Mok, Y.S., 2013. Degradation of veterinary antibiotics by dielectric barrier discharge plasma. *Chem. Eng. J.* 219, 19–27. doi:10.1016/j.cej.2012.12.079.
- Kim, K.S., Kam, S.K., Mok, Y.S., 2015. Elucidation of the degradation pathways of sulfonamide antibiotics in a dielectric barrier discharge plasma system. *Chem. Eng. J.* 271, 31–42. doi:10.1016/j.cej.2015.02.073.
- Kishimoto, N., Morita, Y., Tsuno, H., Oomura, T., Mizutani, H., 2005. Advanced oxidation effect of ozonation combined with electrolysis. *Water Res* 39, 4661–4672.
- Klavarioti, M., Mantzavinos, D., Kassinos, D., 2009. Removal of residual pharmaceuticals from aqueous systems by advanced oxidation processes. *Environ. Int.* 35, 402–417. doi:10.1016/j.envint.2008.07.009.
- Koparal, A.S., Yavuz, Y., Gürel, C., Ögütveren, Ü.B., 2007. Electrochemical degradation and toxicity reduction of C.I. Basic Red 29 solution and textile wastewater by using diamond anode. *J. Hazard. Mater.* 145, 100–108.
- Krýsa, J., Baudys, M., Zlámal, M., Krýsová, H., Morozová, M., Klusoň, P., 2014. Photocatalytic and photoelectrochemical properties of sol-gel TiO₂ films of controlled thickness and porosity. *Catal. Today* 230, 2–7. doi:10.1016/j.cattod.2014.01.008.
- Krause, H., Schweiger, B., Prinz, E., Kim, J., Steinfeld, U., 2011. Degradation of persistent pharmaceuticals in aqueous solutions by a positive dielectric barrier discharge treatment. *J. Electrostat.* 69, 333–338. doi:10.1016/j.elstat.2011.04.011.
- Krishnan, R.Y., Manikandan, S., Subbaiya, R., Biruntha, M., Govarathanan, M., Karmegam, N., 2021. Removal of emerging micropollutants originating from pharmaceuticals and personal care products (PPCPs) in water and wastewater by advanced oxidation processes: A review. *Environ. Technol. Innov.* 23, 101757. doi:10.1016/j.eti.2021.101757.
- Kuo, C.S., Lin, C.F., Hong, P.K.A., 2015. Photocatalytic degradation of methamphetamine by UV/TiO₂-Kinetics, intermediates, and products. *Water Res* 74, 1–9. doi:10.1016/j.watres.2015.01.043.
- Kusic, H., Koprivanac, N., Bozic, A.L., 2006. Minimization of organic pollutant content in aqueous solution by means of AOPs: UV- and ozone-based technologies. *Chem. Eng. J.* 123, 127–137.
- Lí, Q., Lí, Y.W., Wu, P., Xie, R., Shang, J.K., 2008. Palladium Oxide Nanoparticles on Nitrogen-Doped Titanium Oxide: Accelerated Photocatalytic Disinfection

- tion and Post-Illumination Catalytic "Memory. *Adv. Mater.* 20, 3717–3723. doi:10.1002/ADMA.200800685.
- Liao, J., Lin, S., Zhang, L., Pan, N., Cao, X., Li, J., 2012. Photocatalytic degradation of methyl orange using a TiO₂/Ti mesh electrode with 3D nanotube arrays. *ACS Appl. Mater. Interfaces.* 4, 171–177. doi:10.1021/am201220e.
- Liu, Y., Wang, C., Shen, X., Zhang, A., Yan, S., Li, X., Miruka, A.C., Wu, S., Guo, Y., Ogner, S., 2019. Degradation of glucocorticoids in aqueous solution by dielectric barrier discharge: Kinetics, mechanisms, and degradation pathways. *Chem. Eng. J.* 374, 412–428. doi:10.1016/j.cej.2019.05.154.
- Madhu, G.M., Lourdu, M.A., Raj, A., Vasantha, K., Pai, K., 2009. Titanium oxide (TiO₂) assisted photocatalytic degradation of methylene blue. *J. Environ. Biol.* 30, 259–264.
- Magureanu, M., Piroi, D., Mandache, N.B., David, V., Medvedovici, A., Parvulescu, V.I., 2010. Degradation of pharmaceutical compound pentoxifylline in water by non-thermal plasma treatment. *Water Res.* 44, 3445–3453. doi:10.1016/j.watres.2010.03.020.
- Magureanu, M., Piroi, D., Mandache, N.B., David, V., Medvedovici, A., Bradu, C., Parvulescu, V.I., 2011. Degradation of antibiotics in water by non-thermal plasma treatment. *Water Res.* 45, 3407–3416. doi:10.1016/j.watres.2011.03.057.
- Magureanu, M., Piroi, D., Mandache, N.B., David, V., Medvedovici, A., Bradu, C., Parvulescu, V.I., 2011. Degradation of antibiotics in water by non-thermal plasma treatment. *Water Res.* 45, 3407–3416. doi:10.1016/j.watres.2011.03.057.
- Magureanu, M., Dobrin, D., Mandache, N.B., Bradu, C., Medvedovici, A., Parvulescu, V.I., 2013. The mechanism of plasma destruction of enalapril and related metabolites in water. *Plasma Process. Polym.* 10, 459–468. doi:10.1002/ppap.201200146.
- Magureanu, M., Bilea, F., Bradu, C., Hong, D., 2021. A review on non-thermal plasma treatment of water contaminated with antibiotics. *J. Hazard. Mater.* 417. doi:10.1016/j.jhazmat.2021.125481.
- Malik, M.A., 2010. Water purification by plasmas: Which reactors are most energy efficient? *Plasma Chem. Plasma Process.* 30, 21–31. doi:10.1007/s11090-009-9202-2.
- Maness, P.C., Smolinski, S., Blake, D.M., Huang, Z., Wolfrum, E.J., Jacoby, W.A., 1999. Bactericidal activity of photocatalytic TiO₂ reaction: Toward an understanding of its killing mechanism. *Appl. Environ. Microbiol.* 65, 4094–4098. doi:10.1128/AEM.65.9.4094-4098.1999.
- Massima Mouele, E.S., Fatoba, O.O., Babajide, O., Badmus, K.O., Petrik, L.F., 2018. Review of the methods for determination of reactive oxygen species and suggestion for their application in advanced oxidation induced by dielectric barrier discharges. *Environ. Sci. Pollut. Res.* 25, 9265–9282. doi:10.1007/s11356-018-1392-9.
- E.S. Massima Mouele, J.O. Tijani, M. Masikini, O.O. Fatoba, C.P. Eze, C.T. Onwordi, M.T. Zar Myint, H.H. Kyaw, J. Al-Sabahi, M. Al-Abri, S. Dobretsov, K. Laatikainen, L.F. Petrik, Spectroscopic Measurements of Dissolved O₃, H₂O₂ and OH Radicals in Double Cylindrical Dielectric Barrier Discharge Technology: Treatment of Methylene Blue Dye Simulated Wastewater, *Plasma.* 3 (2020) 59–91. doi:10.3390/plasma3020007.
- Massima Mouele, E.S., Tijani, J.O., Badmus, K.O., Perea, O., Babajide, O., Zhang, C., Shao, T., Sosnin, E., Tarasenko, V., Fatoba, O.O., Laatikainen, K., Petrik, L.F., 2021. Removal of pharmaceutical residues from water and wastewater using dielectric barrier discharge methods—a review. *Int. J. Environ. Res. Public Health.* 18, 1–42. doi:10.3390/ijerph18041683.
- Matsunaga, T., Tomoda, R., Nakajima, T., Wake, H., 1985. Photoelectrochemical sterilization of microbial cells by semiconductor powders. *FEMS Microbiol. Lett.* 29, 211–214. doi:10.1111/J.1574-6968.1985.TB00864.X.
- Merajin, M.T., Sharifnia, S., Hosseini, S.N., Yazdanpour, N., 2013. Photocatalytic conversion of greenhouse gases (CO₂ and CH₄) to high value products using TiO₂ nanoparticles supported on stainless steel webnet. *J. Taiwan Inst. Chem. Eng.* 44, 239–246. doi:10.1016/j.jtice.2012.11.007.
- Mhuka, V., Dube, S., Nindi, M.M., 2020. Occurrence of pharmaceutical and personal care products (PPCPs) in wastewater and receiving waters in South Africa using LC-Orbitrap™ MS. *Emerg. Contam.* 6, 250–258. doi:10.1016/j.emcon.2020.07.002.
- Mhuka, V., Dube, S., Nindi, M.M., 2020. Occurrence of pharmaceutical and personal care products (PPCPs) in wastewater and receiving waters in South Africa using LC-Orbitrap™ MS. *Emerg. Contam.* 6, 250–258. doi:10.1016/J.EMCON.2020.07.002.
- Miruka, A.C., Zhang, A., Wang, Q., Zhu, D., Wang, Z., Sun, Z., Héroux, P., Liu, Y., 2021. Degradation of glucocorticoids in water by a synergistic system of peroxy-monosulfate, microbubble and dielectric barrier discharges. *J. Water Process Eng.* 42. doi:10.1016/j.jwpe.2021.102175.
- Mishra, K.P., Gogate, P.R., 2010. Intensification of degradation of Rhodamine B using hydrodynamic cavitation in the presence of additives. *Sep. Purif. Technol.* 75, 385–391.
- Mouele, E.S.M., Tijani, J.O., Fatoba, O.O., Petrik, L.F., 2015. Degradation of organic pollutants and microorganisms from wastewater using different dielectric barrier discharge configurations—a critical review. *Environ. Sci. Pollut. Res.* 22, 18345–18362. doi:10.1007/s11356-015-5386-6.
- E.S.M. Mouele, M. Dinu, F. Cummings, O.O. Fatoba, M.T.Z. Myint, H.H. Kyaw, A.C. Parau, A. Vladescu, M.G. Francesconi, S. Pescetelli, A. Di Carlo, A. Agresti, M. Al-Abri, S. Dobretsov, M. Braic, L.F. Petrik, Effect of calcination time on the physicochemical properties and photocatalytic performance of carbon and nitrogen co-doped TiO₂ nanoparticles, *Catalysts.* 10 (2020). doi:10.3390/catal10080847.
- Mouele, E.S.M., Dinu, M., Parau, A.C., Vladescu, A., Myint, M.T.Z., Kyaw, H.H., Al-Sabahi, J., Al-Abri, M., Dobretsov, S., Al Belushi, M.A., Al-Mamari, R., Braic, M., Petrik, L.F., 2020a. Anticorrosion coated stainless steel as durable support for c-n-tio2 photo catalyst layer. *Materials (Basel)* 13, 1–27. doi:10.3390/ma13194426.
- Mouele, E.S.M., Ngqoloda, S., Pescetelli, S., Di Carlo, A., Dinu, M., Vladescu, A., Parau, A.C., Agresti, A., Braic, M., Arendse, C.J., Petrik, L.F., 2020b. Spin coating immobilisation of c-n-tio2 co-doped nano catalyst on glass and application for photocatalysis or as electron transporting layer for perovskite solar cells. *Coatings* 10, 1–24. doi:10.3390/coatings10111029.
- Mouele, E.S.M., Tijani, J.O., Badmus, K.O., Perea, O., Babajide, O., Fatoba, O.O., Zhang, C., Shao, T., Sosnin, E., Tarasenko, V., Laatikainen, K., Petrik, L.F., 2021. A critical review on ozone and co-species, generation and reaction mechanisms in plasma induced by dielectric barrier discharge technologies for wastewater remediation. *J. Environ. Chem. Eng.* 9.
- Mouele, E.S.M., Tijani, J.O., Badmus, K.O., Perea, O., Babajide, O., Fatoba, O.O., Zhang, C., Shao, T., Sosnin, E., Tarasenko, V., Laatikainen, K., Petrik, L.F., 2021. A critical review on ozone and co-species, generation and reaction mechanisms in plasma induced by dielectric barrier discharge technologies for wastewater remediation. *J. Environ. Chem. Eng.* 9. doi:10.1016/j.jece.2021.105758.
- Moza, S., Tomaszewska, M., Morawski, A.W., 2005. Photocatalytic degradation of azo-dye Acid Red 18. *Desalination* 185, 449–456.
- Nakagawa, Y., Mitamura, S., Fujiwara, Y., Nishitani, T., 2003. Decolorization of rhodamine B in water by pulsed high-voltage gas discharge. *Japanese J. Appl. Physics, Part 1 Regul. Pap. Short Notes Rev. Pap.* 42, 1422–1428. doi:10.1143/jjap.42.1422.
- Nam, S., Renganathan, V., Tratnyek, P.G., 2001. Substituent effects on azo dye oxidation by the FeIII-EDTA-H₂O₂ system. *Chemosphere* 45, 59–65.
- Nifuku, M., Horvath, M., Bodnár, J., Zhang, G., Tanaka, T., Kiss, E., Woynfirovich, G., Katoh, H., 1997. A study on the decomposition of volatile organic compounds by pulse corona. *J. Electroanal. Chem.* 40, 687–692.
- Olatunde, O.C., Kuwarega, A.T., Onwujiwe, D.C., 2020. Photo enhanced degradation of contaminants of emerging concern in waste water. *Emerg. Contam.* 6, 283–302. doi:10.1016/j.emcon.2020.07.006.
- Omakli, O.C., Yazıcı, M., Yetim, T., Yetim, A.F., Çomaklı, O., Çelik, A., 2015. The effect of calcination temperatures on structural and electrochemical properties of TiO₂ film deposited on commercial pure titanium. *Surf. Coat. Technol.* doi:10.1016/j.surfcoat.2015.11.055.
- Patil, A.D., Baral, S.S., Dhanke, P.B., Madankar, C.S., Patil, U.S., Kore, V.S., 2018. Parametric studies of methyl esters synthesis from Thumba seed oil using heterogeneous catalyst under conventional stirring and ultrasonic cavitation. *Mater. Sci. Energy Technol.* 1, 106–116.
- A. Patil, S.S. Baral, P. Dhanke, V. Kore, Biodiesel production using prepared novel surface functionalised TiO₂ nano-catalyst in hydrodynamic cavitation reactor, *Mater. Today Proc.* 27 (2020) 198–203. doi:10.1016/j.matpr.2019.10.009.
- C. Qi, X. Liu, C. Lin, X. Zhang, J. Ma, H. Tan, W. Ye, Degradation of sulfamethoxazole by microwave-activated persulfate: Kinetics, mechanism and acute toxicity, (2014). doi:10.1016/j.cej.2014.03.086.
- qiong Gao, Y., Yun Gao, N., Deng, Y., qiong Yang, Y., Ma, Y., 2012. Ultraviolet (UV) light-activated persulfate oxidation of sulfamethazine in water. *Chem. Eng. J.* 195–196, 248–253. doi:10.1016/j.cej.2012.04.084.
- Ren, R., Wen, Z., Cui, S., Hou, Y., Guo, X., Chen, J., 2015. Controllable Synthesis and Tunable Photocatalytic Properties of Ti³⁺-doped TiO₂. *Sci. Reports* 5 (5), 1–11. doi:10.1038/srep10714, 2015.
- Rong, S.P., Sun, Y.B., Zhao, Z.H., 2014. Degradation of sulfadiazine antibiotics by water falling film dielectric barrier discharge. *Chinese Chem. Lett.* 25, 187–192. doi:10.1016/j.ccl.2013.11.003.
- Rong, S., Sun, Y., Zhao, Z., Wang, H., 2014. Dielectric barrier discharge induced degradation of diclofenac in aqueous solution. *Water Sci. Technol.* 69, 76–83. doi:10.2166/wst.2013.554.
- Sang, W., Cui, J., Feng, Y., Mei, L., Zhang, Q., Li, D., Zhang, W., 2019. Degradation of aniline in aqueous solution by dielectric barrier discharge plasma: Mechanism and degradation pathways. *Chemosphere* 223, 416–424. doi:10.1016/j.chemosphere.2019.02.029.
- Shu, H.Y., Huang, C.R., 1995. Degradation of commercial azo dyes in water using ozonation and UV enhanced ozonation process. *Chemosphere* 31, 3813–3825.
- Souzanchi, S., Vahabzadeh, F., Fazel, S., Hosseini, S.N., 2013. Performance of an Annular Sieve-Plate Column photoreactor using immobilized TiO₂ on stainless steel support for phenol degradation. *Chem. Eng. J.* 223, 268–276. doi:10.1016/j.cej.2013.02.123.
- Spadaro, J.T., Gold, M.H., Renganathan, V., 1992. Degradation of azo dyes by the lignin-degrading fungus *Phanerochaete chrysosporium*. *Appl. Environ. Microbiol.* 58, 2397–2401. doi:10.1128/AEM.58.8.2397-2401.1992.
- Staelin, J.; Hinge, J., 'Decomposition of ozone in water in the presence of organic solutes acting as promoters and inhibitors of radical chain reactions,' *Environ. Sci. Technol.* 19 (1985) 1206–1213. doi:10.1021/es00142a012.
- Suzuki, T., Timofei, S., Kurunczi, L., Dietze, U., Schüürmann, G., 2001. Correlation of aerobic biodegradability of sulfonated azo dyes with the chemical structure. *Chemosphere* 45, 1–9.
- Tijani, J.O., Mouele, M.E.S., Tottito, T.C., Fatoba, O.O., Petrik, L.F., 2017. Degradation of 2-Nitrophenol by Dielectric Barrier Discharge System: The Influence of Carbon Doped TiO₂ Photocatalyst Supported on Stainless Steel Mesh. *Plasma Chem. Plasma Process.* 37, 1343–1373. doi:10.1007/s11090-017-9824-8.
- Tijani, J.O., Mouele, M.E.S., Fatoba, O.O., Babajide, O.O., Petrik, L.F., 2017. Degradation of bisphenol-A by dielectric barrier discharge system: Influence of polyethylene glycol stabilized nano zero valent iron particles. *Adv. Nat. Sci. Nanosci. Nanotechnol.* 8. doi:10.1088/2043-6254/aa7714.
- A.U. Tri Sugiarto, M. Sato, Pulsed plasma processing of organic compounds in aqueous solution, 2001.
- A.G. Trovó, R.F.P. Nogueira, A. Agüera, C. Sirtori, A.R. Fernández-Alba, Photodegradation of sulfamethoxazole in various aqueous media: Persistence, toxicity and photoproducts assessment, *Chemosphere.* 77 (2009) 1292–1298. doi:10.1016/j.chemosphere.2009.09.065.
- Wang, X., Wang, J., Guo, P., Guo, W., Wang, C., 2009. Degradation of rhodamine B in aqueous solution by using swirling jet-induced cavitation combined with H₂O₂. *J. Hazard. Mater.* 169, 486–491.
- Wang, X., Jia, J., Wang, Y., 2010. Electrochemical degradation of reactive dye in the presence of water jet cavitation. *Ultrason. Sonochem.* 17, 515–520.

- Wang, A., Li, Y.Y., Estrada, A.L., 2011. Mineralization of antibiotic sulfamethoxazole by photoelectro-Fenton treatment using activated carbon fiber cathode and under UVA irradiation. *Appl. Catal. B Environ.* 102, 378–386. doi:10.1016/j.apcatb.2010.12.007.
- Y. Wang, X. Liao, Y. Luo, Q. Yang, G. Li, Influence of Surface-functionalized Graphene Oxide on the Cell Morphology of Poly(methyl methacrylate) Composite, (2015). doi:10.1016/j.jmst.2015.01.010.
- Wang, M., Han, J., Hu, Y., Guo, R., Mesoporous, C., 2017. N-codoped TiO₂ hybrid shells with enhanced visible light photocatalytic performance. *RSC Adv* 7, 15513–15520. doi:10.1039/c7ra00985b.
- Wardenier, N., Vanraes, P., Nikiforov, A., Van Hulle, S.W.H., Leys, C., 2018. Title: Removal of micropollutants from water in a continuous-flow electrical discharge reactor Removal of micropollutants from water in a continuous-flow electrical discharge reactor. *J. Hazard. Mater.* doi:10.1016/j.jhazmat.2018.08.095.
- Wardenier, N., Liu, Z., Nikiforov, A., Van Hulle, S.W.H., Leys, C., 2019. Micropollutant elimination by O₃, UV and plasma-based AOPs: An evaluation of treatment and energy costs. *Chemosphere* 234, 715–724. doi:10.1016/j.chemosphere.2019.06.033.
- Wu, D., Wang, L., 2013. Low-temperature synthesis of anatase C-N-TiO₂ photocatalyst with enhanced visible-light-induced photocatalytic activity. *Appl. Surf. Sci.* 271, 357–361. doi:10.1016/j.apsusc.2013.01.202.
- Xiao, G., Zhang, X., Zhang, W., Zhang, S., Su, H., Tan, T., 2015. Visible-light-mediated synergistic photocatalytic antimicrobial effects and mechanism of Ag-nanoparticles@chitosan-TiO₂ organic-inorganic composites for water disinfection. *Appl. Catal. B Environ.* 170–171, 255–262. doi:10.1016/j.apcatb.2015.01.042.
- Xu, Z., Xue, X., Hu, S., Li, Y., Shen, J., Lan, Y., Zhou, R., Yang, F., Cheng, C., 2020. Degradation effect and mechanism of gas-liquid phase dielectric barrier discharge on norfloxacin combined with H₂O₂ or Fe²⁺. *Sep. Purif. Technol.* 230. doi:10.1016/j.seppur.2019.115862.
- J.H. Yan, C.M. Du, X.D. Li, B.G. Cheron, M.J. Ni, K.F. Cen, Degradation of Phenol in Aqueous Solutions by Gas-Liquid Gliding Arc Discharges, 26 (2006). doi:10.1007/s11090-005-8723-6.
- Yetim, T., 2016. Corrosion Behavior of Ag-doped TiO₂ Coatings on Commercially Pure Titanium in Simulated Body Fluid Solution. *J. Bionic Eng.* 13, 397–405. doi:10.1016/S1672-6529(16)60311-6.
- yi Pan, X., chen Qiao, X., 2019. Influences of nitrite on paracetamol degradation in dielectric barrier discharge reactor. *Ecotoxicol. Environ. Saf.* 180, 610–615. doi:10.1016/j.ecoenv.2019.04.037.
- Zhang, J., Xing, Z., 2018. J. Cui, Z. Li, S. Tan, J. Yin, J. Zou, Q. Zhu, W. Zhou, C. N co-doped porous TiO₂ hollow sphere visible light photocatalysts for efficient removal of highly toxic phenolic pollutants. *Dalt. Trans.* 47, 4877–4884. doi:10.1039/c8dt00262b.
- Zhang, L., Zhu, Y., He, Y., Li, W., Sun, H., 2003. Preparation and performances of mesoporous TiO₂ film photocatalyst supported on stainless steel. *Appl. Catal. B Environ.* 40, 287–292.
- Zhang, X., Li, D., Wan, J., Yu, X., 2016. Preparation of Ti mesh supported N-S-C-tridoped TiO₂ nanosheets to achieve high utilization of optical energy for photocatalytic degradation of norfloxacin. *RSC Adv* 6, 17906–17912. doi:10.1039/c5ra27639j.
- Zhang, Y., Liu, X., Wang, Y., Jiang, P., Quek, S.Y., 2016. Antibacterial activity and mechanism of cinnamon essential oil against *Escherichia coli* and *Staphylococcus aureus*. *Food Control* 59, 282–289. doi:10.1016/j.foodcont.2015.05.032.
- Zhang, G., Sun, Y., Zhang, C., Yu, Z., 2017. Decomposition of acetaminophen in water by a gas phase dielectric barrier discharge plasma combined with TiO₂-rGO nanocomposite: Mechanism and degradation pathway. *J. Hazard. Mater.* 323, 719–729. doi:10.1016/j.jhazmat.2016.10.008.